TECHNICAL UNIVERSITY OF CRETE

SCHOOL OF ELECTRICAL AND COMPUTER ENGINEERING

Study of Dielectric Strength of High Voltage Cables

Diploma Thesis

Georgios Messaritakis

Thesis Committee:

Georgios Peppas, Assistant Professor – Thesis Supervisor

Konstantinos Gyftakis, Associate. Professor

Eftychios Koutroulis, Professor

July 2025

ABSTRACT

Reliable dielectric performance of high voltage (HV) cables is critical for power system integrity, yet the outer oversheath can present unexpected weaknesses during lightning transient events. This thesis undertakes a thorough investigation of dielectric strength in two extruded HV cable constructions—a 150 kV AL/XLPE/SWAS/PE design and a 110 kV N2XS(F)2Y variant—focusing on the cables' oversheath behavior under impulse voltage stress. International test protocols (IEC and ASTM) that guide specimen preparation, measurement, and testing were used.

Initial evaluation revealed that factory-applied semiconductive jacket layers often exceed the thin screening film assumed in standards, creating thicknesses on the order of millimeters and resulting in small surface resistances in the kiloohm range. Such oversheath characteristics led to surface conduction and creepage discharge when applying lightning impulses, visibly carbonizing the oversheath and producing distorted waveforms with abnormally rapid tail decay and erratic discharge paths. Mechanical removal of these semiconductive layers—achieved by rasping, after abrasion proved insufficient—restored insulation surfaces to GΩ-range resistivity, eliminating leakage paths and enabling correct 1.2/50 μs waveform generation during oil-immersed impulse tests. Clean electrode installation and controlled immersion protocols ensured reproducible conditions.

For the 150 kV cable, only after complete removal of the multi-millimeter semiconductive oversheath did the impulse waveforms conform to IEC tolerances and the insulation exhibit clean puncture breakdown without lateral tracking. Similar findings are true for the 110 kV cable, where surface-resistance verification and targeted layer removal preceded successful impulse withstand tests.

Experimental container design also evolved through prototypes to address mechanical failures under high-stress impulses, culminating in a nested, oil-filled assembly that maintained dielectric clearance and structural integrity during repetitive testing. The Marx generator was analyzed, modified to a single-stage impulse voltage generator for lower voltage impulses. The produced waveforms were validated via simulations and measurements.

This work studies the dielectric strength, providing detailed procedures for oversheath assessment, mechanical removal techniques, electrode assembly, oil-immersion setup, and impulse voltage application. Finally, this study can contribute empirical dielectric-strength limits under transient stresses, supporting improved testing protocols and cable design and production evaluations.

Keywords: ASTM standards, dielectric strength, high voltage cable, IEC standards, impulse voltage testing, Marx generator, oil immersion, oversheath weak points, semiconductive oversheath, surface discharge, XLPE insulation.

ACKNOWLEDGEMENTS

I would like to express my sincere gratitude to my supervisor, Georgios Peppas, for his continuous support, guidance, and encouragement throughout this thesis. His expertise, patience, and insightful feedback have been instrumental in shaping both the direction and depth of this work. I am also grateful to the faculty and staff of the Electrical and Computer Engineering at Technical University of Crete for providing the necessary resources and a stimulating research environment that allowed me to explore and refine my ideas effectively.

A special thanks goes to Michail Pitsikalis. His generous assistance, willingness to discuss problems in depth, and practical advice on experimental and analytical techniques greatly facilitated my progress. Michail's support—both technical and motivational—has been a tremendous help throughout this process.

I am especially thankful to the family of Elemko for generously providing access to their laboratory facilities and for the hands-on guidance that was crucial to completing the experimental aspects of this study. Their trust and willingness to share resources made possible many of the practical components of my research, and the mentorship I received there greatly enriched my academic journey.

I also wish to acknowledge the valuable contributions of Mr. Nikolaos Kokkinos, Evangelos Senis, and Giannis Koutsoubis. Their expertise, thoughtful discussions, and constructive suggestions have significantly improved various parts of this study. Whether through help with data interpretation, methodological advice, or moral support during challenging phases, their involvement has been invaluable.

I am also grateful to Athina Antoniou, who conducted her thesis alongside mine. Her companionship throughout this journey, the shared discussions about methodologies, and the mutual encouragement during challenging moments have been very meaningful. Having Athina alongside has made this process more collaborative and motivating.

My deepest thanks go to my family and friends for their unwavering support and understanding. To my family: your belief in me, patience during late nights and busy weekends, and constant encouragement have given me the strength to persevere. To my friends: thank you for the laughter, timely distractions, and motivational pep talks that helped me maintain balance and perspective throughout this demanding process.

Lastly, I am grateful to my fellow colleagues and the broader research community for inspiring conversations, helpful feedback, and collaboration. Every discussion—formal or informal—has contributed in its own way to the ideas and improvements in this thesis.

Thank you all for being part of this journey; your support has made this achievement possible.

TABLE OF CONTENTS

FIGURES LIST

TABLES LIST

CHAPTER 1: INTRODUCTION

1.1 General Overview

High voltage power cables are critical components within electrical energy transmission networks, tasked with safely conducting large amounts of electrical energy over considerable distances. A crucial but often underestimated component of these cables is the insulation oversheath, which serves as a protective outer layer. This oversheath provides essential mechanical protection against external stresses, moisture ingress, and environmental contaminants, as well as supplemental electrical insulation. Despite its importance, the dielectric integrity of the cable, oversheath—particularly under impulse voltage stress—is frequently assumed sufficient by existing manufacturing practices and international standards. However, operational evidence has suggested potential weaknesses in the cable jackets, especially when exposed to transient conditions that may significantly differ from the conditions anticipated by standardized tests.

1.2 State of the Art

Most of the existing research and standards in high voltage cable technology emphasize testing and validating primary insulation systems, often relegating the jacket's dielectric performance to a secondary consideration. Standards such as IEC and ASTM primarily outline routine tests focused on jacket thickness, mechanical durability, and general electrical insulation, without extensive guidelines specific to impulse voltage stress. Consequently, literature explicitly dedicated to the detailed analysis and characterization of oversheath insulation under impulse voltage conditions remains limited. This gap has resulted in insufficient recognition of jacket vulnerabilities under realistic transient events, leaving manufacturers and operators potentially unaware of significant risks related to premature breakdown and subsequent cable failures.

1.3 Thesis Objective

The principal objective of this thesis is to explicitly expose and systematically document the dielectric weaknesses of the insulation oversheaths of high-voltage cables under impulse voltage testing conditions. Specifically, the thesis aims to:

- Evaluate the dielectric breakdown characteristics of cable oversheaths, identifying their performance limitations relative to rated operational voltages.
- Demonstrate how hidden or poorly documented production aspects, such as semiconductive layers in jackets, exacerbate impulse voltage breakdown phenomena.
- Provide quantitative evidence of the jacket breakdown occurring at voltages significantly below the cable's nominal operational rating, highlighting inadequacies in current standard assumptions.

The thesis will try these objectives through controlled laboratory experiments, meticulous specimen preparation, impulse voltage testing, and detailed post-test analysis, offering critical insights into the dielectric limitations and underlying production-related flaws of high-voltage cable oversheaths.

1.4 Contribution

The thesis will further deepen the understanding of dielectric vulnerabilities within cable oversheath materials under lightning transients, addressing a typically overlooked, yet critical gap of current standards and common manufacturing practices. The core scientific and practical contributions of the thesis are summarized as follows:

- Empirical identification and documentation of jacket insulation breakdown at impulse voltage levels (80–90 kV) significantly below the rated nominal voltage, clearly demonstrating inherent jacket weaknesses.
- Highlighting previously overlooked issues arising from semiconductive layers embedded within jacket materials, which severely degrade dielectric performance under impulse stress.

- Development and validation of specific mechanical removal methods for problematic semiconductive layers to ensure accurate dielectric strength assessments and consistent test conditions.
- Providing critical experimental data and analytical insights to inform future updates in international standards and manufacturing guidelines, emphasizing enhanced quality control and more rigorous impulse testing protocols specifically targeting jacket materials.

Through these contributions, the thesis aims to provoke meaningful improvements in cable manufacturing, testing practices, and standardization efforts, ultimately enhancing the reliability and operational safety of high-voltage cable systems.

CHAPTER 2: LITERATURE REVIEW

2.1 Introduction

In high voltage (HV) and medium voltage (MV) power systems, cables serve as indispensable components for the transmission and distribution of electrical energy. Their operational reliability directly impacts the stability and efficiency of electrical power systems, making the design and performance of these cables critical. Among the various characteristics of a power cable, the dielectric properties of the inner insulation and the outer sheath (oversheath) are essential in ensuring safe and efficient operation under operating and transient conditions. Particularly power cables must endure continuous operational stresses, transient overvoltages, and exposure to environmental factors without failure. These conditions place stringent requirements on their materials and design [1].

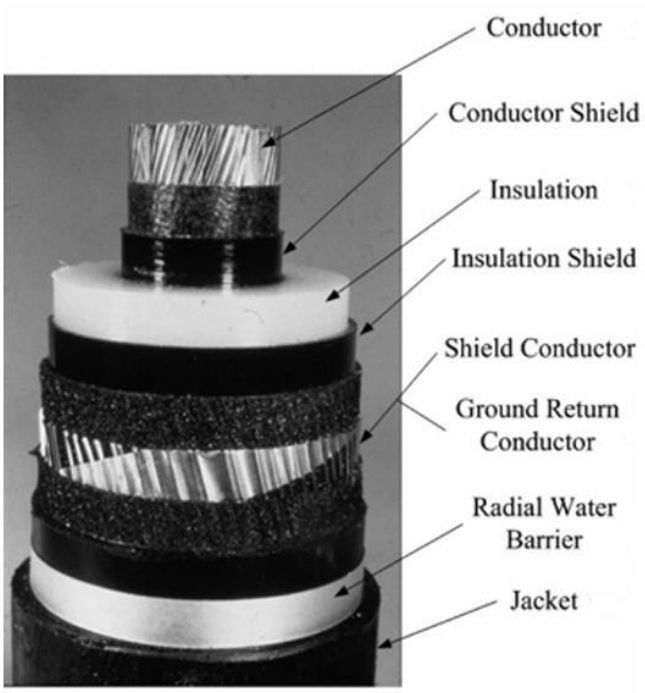

Figure 1. Components of high voltage cable [1].

The central copper or aluminum core in a HV cable is engineered to conduct the rated current with minimal resistive losses, its purity and cross-section tailored to balance ampacity against Joule losses (I^2R) heating. In modern extruded-dielectric designs the strands are compacted into a round-sector profile, reducing voids and achieving an optimal geometric mean radius for enhanced electrical and thermal performance. These conductors must meet strict DC resistance and AC skin-effect loss criteria under both continuous and fault conditions [1].

The conductor is encased with a thin semiconducting layer—usually a carbon-loaded EPDM compound—extruded directly onto the strands to smooth microscopic surface irregularities and create a uniform equipotential boundary. This semiconductive layer adheres closely to the metal, preventing space-charge accumulation and local field intensification that could trigger partial discharges and reduce the life span of the power cable [1].

Over the semiconducting shields, a metallic sheath—usually composed of copper or aluminum tapes or wires or both—provides a low-resistance path for charging and fault currents while containing the electrostatic field within the cable. In fluid-filled variants this sheath also serves as a pressure enclosure; in extruded designs it helps block moisture ingress and adds mechanical protection against soil movement and impact [1].

The primary dielectric layer is the inner insulation. This layer is designed to withstand electrical, thermal and mechanical stresses precipitated by nominal operation conditions and transient events; such are switching or lightning surges. Its primary function is to preclude electrical breakdown. The dielectric strength of the inner insulation is a decisive factor in cable design. Any failure can potentially lead to catastrophic consequences, including system blackouts and equipment damage. To prevent any failure due to poor design and to verify the inner insulation’s design, standardized tests are used to evaluate the insulation under a variety of electrical stresses, including AC, DC, and high-frequency impulse voltages. In addition to the dielectric withstand, the insulation's response to aging and thermally induced effects should be tested to ensure its long-term functioning [1].

The outer sheath, also referred to as oversheath, is often perceived primarily as a mechanical barrier, however, it also serves as an essential dielectric barrier. It protects the cable from external environmental influences, such as moisture ingress, chemical exposure, and mechanical abrasion. In certain applications, especially in underground or subsea environments, the oversheath must

demonstrate robust environmental properties to prevent degradation under high humidity, soil resistivity, or mechanical stress. Thus, its overall performance is a critical determinant of the cable's reliability and durability [1].

The test procedure and design verification of power cables is guided by international standards developed by organizations such as the International Electrotechnical Commission (IEC), Institute of Electrical and Electronics Engineers (IEEE), Conseil International des Grands Réseaux Electriques (Cigre) and American Society for Testing and Material (ASTM). These standards define a hierarchy of testing protocols:

- **Type Tests**: Performed to validate the cable's compliance with design and performance specifications, often conducted during the development phase.
- **Routine Tests**: Performed on every cable, or some indicative samples per manufactured cable batch to ensure consistent production quality.
- **Special Tests**: Performed to ensure conformity to extreme conditions or specific operational scenarios. Usually, they are requested by clients.

Each test category is performed at different stages of product development or production. Each test, regardless of the category of tests that is implemented, addresses distinct aspects of performance, providing a comprehensive assessment framework. For example, AC voltage tests can be either a type or routine test. In both cases, the test's purpose is to examine the insulation's ability to withstand electrical stress.

2.2 Type Tests

Inner insulation

Voltage test: Before conducting any electrical type tests, the insulation thickness of the cable must be measured using a measuring instrument with a magnification of at least 10 times. For accurate measurements, a digital image analyzer should also be utilized. These two kinds of machinery will enable a measurement with precision of 0.01 mm. For the thickness measurement any covering must be removed from the insulation, and the conductor(s), along with any separator,

should be withdrawn carefully to prevent any damages of the insulation. If the semi-conducting inner or outer layers are attached to the insulation, they should not be removed.

Each test sample must be a thin slice of insulation. This slice should be cut using an appropriate tool along a plane that is perpendicular to the conductor's longitudinal axis. The cores of flat cables, that are not sheathed, must remain intact. In case the insulation has an indented marking, which results in a localized reduction in thickness, the sample should be taken to include this marking. The test specimen must be positioned beneath the measuring apparatus, in order to orient the cut surface perpendicular to the optical axis. In instances where the internal profile of the specimen is circular, six radial measurements should be taken at approximately 60° intervals, as illustrated in Figure 2. For cores that are sector-shaped, the same number of measurements should be conducted as depicted in Figure 3. When insulation is removed from a stranded conductor, six radial measurements are to be performed, following the guidance provided in Figure 4 and Figure 5. In cases where the outer profile exhibits irregularities, measurements should be executed as indicated in Figure 6. In situations where such screening layers are present beneath or above opaque insulation, a measuring microscope is required for accurate assessment. For flat non-sheathed cables, measurements should adhere to the methodology shown in Figure 7, with the insulation thickness in the direction of the adjacent core calculated as half the distance between the conductors.

In all scenarios, the initial measurement should be taken at the point where the insulation is thinnest. However, any indented markings on the insulation should not be factored into the calculations for mean thickness. Nonetheless, the thickness at the location of the indented marking must meet the minimum requirements outlined in the applicable standard. Measurements should be recorded in millimeters, with two decimal places for specified thicknesses of 0.5 mm or greater, and three decimal places for thicknesses below 0.5 mm. This measurement is to ensure that the average thickness does not significantly exceed the nominal value. If the average insulation thickness is no more than 5% greater than the nominal value, the test voltages should correspond to the values indicated in Table 2 for the cable's rated voltage. If the average insulation thickness is greater than the nominal value by more than 5% but not exceeding 15%, the test voltage should be calibrated to produce an electrical stress on the conductor screen that corresponds to the level present when the average insulation thickness matches the nominal value, using the standard test

voltages defined for the cable's rated voltage. The cable length utilized for the electrical type tests must not have an average insulation thickness that surpasses the nominal value by more than 15%.

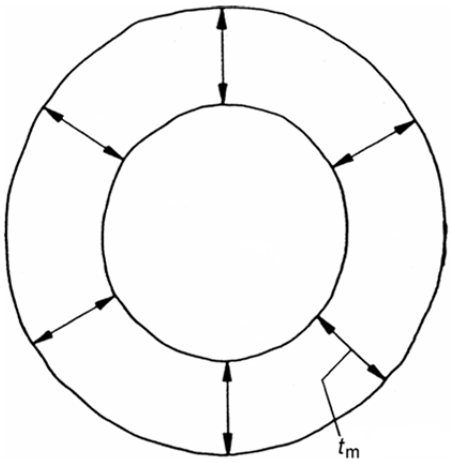

Figure 2. Measurement of insulation (circular inner profile) [2].

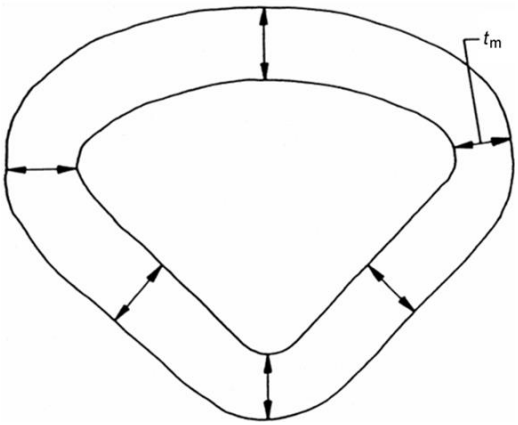

Figure 3. Measurement of insulation thickness (sectoral-shaped conductor) [2].

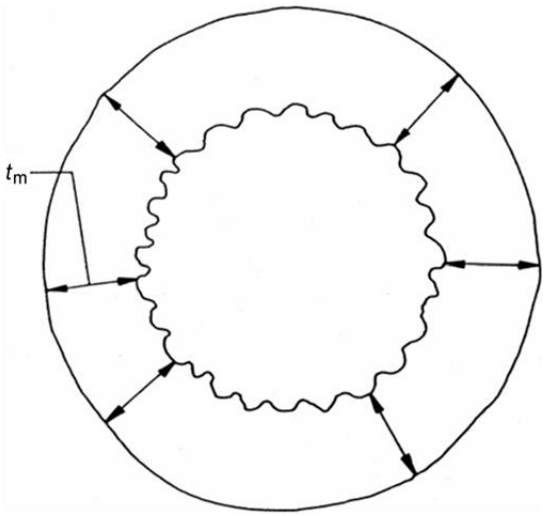

Figure 4. Measurement of insulation thickness (stranded conductor) [2].

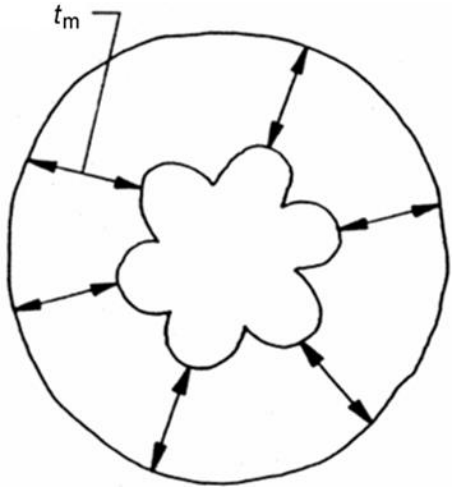

Figure 5. Measurement of insulation thickness (stranded conductor) [2].

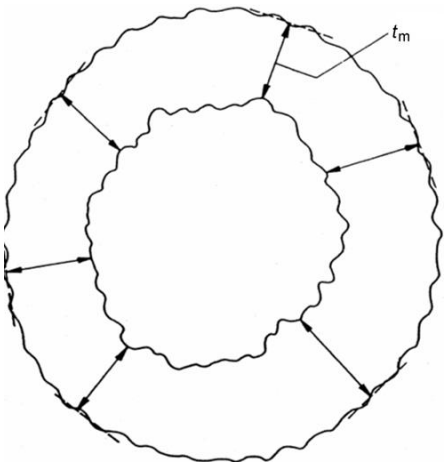

Figure 6. Measurement of insulation thickness (uneven outer profile) [2].

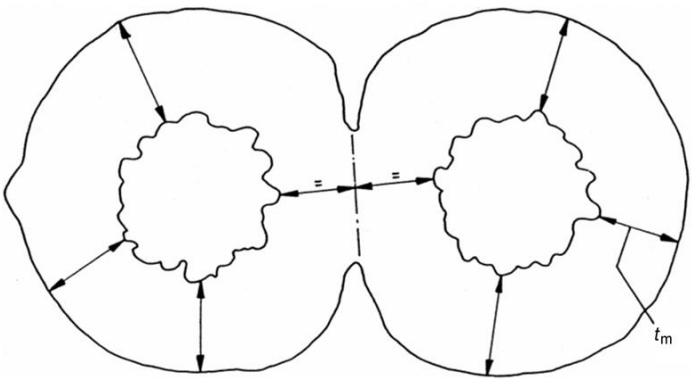

Figure 7. Measurement of insulation thickness (twin flat non-sheathed cable) [2].

Tan δ measurement: Before the test, the conductor must reach temperature in the range of 5 K to 10 K above the peak temperature of nominal operation, using conductor current only. The conductor temperature can be measured by measuring its resistance or using sensors on the metallic sheath or by means of temperature sensors on the conductor of another, similar sample of the same cable heated by the same means. After ensuring the temperature has reached its desired value, tan δ is measured using the power frequency voltage U_0 as specified in Table 2. The permissible limits of the measurement are tabulated in Table 1 [3].

Table 1. Tan δ per material [3].

Designation of compound (see 4.2)	**PE**	**HDPE**	**EPR/HEPR**	**XLPE**
Maximum tan δ (10^{-4})	10	10	50	10

Lightning Impulse Voltage Test: The assembly must be heated with conductor current only, similarly to the tan δ measurement, until it reaches the range of 5 K to 10 K higher temperature than the temperature of the nominal operation. After the temperature has reached the desired limits, it should be maintained for, at least, 2 hours. If the desired temperature can't be reached, then an additional insulation layer should be added. The test voltage applied to the sample is defined in Table 2, column 8 and the lightning impulse voltage must have time to front T_1 = 1 to 5 μs and time to half 50 μs. The tolerances for these parameters are defined in IEC 60060-1. The unit under test should handle without problem (failure or flashover) 10 positive and 10 negative impulses of the referred value [3], [4], [5].

Power Frequency Voltage Test: Following the lightning impulse voltage test, the assembly should undergo a 15-minute power frequency voltage test at 2.5 U_0, per Table 2, column 9. It is left at the manufacturer's discretion, whether this test is performed during the cooling period or at ambient temperature. The pass criterion of this test is that no insulation breakdown or flashover should occur [3].

Testing Based on ASTM D149-09:

The ASTM D149-09 standard outlines a comprehensive approach for evaluating the dielectric strength of solid insulating materials. The process begins with the meticulous preparation of the specimens to ensure consistency and reliability of the results. Samples are selected and prepared to meet specific geometric and surface quality requirements; their surfaces must be smooth, parallel, and free of defects to prevent irregular electric field distributions during testing. Sample size is chosen to minimize the risk of flashover, with larger specimens used for thin materials to enable multiple tests on the same sample. For thicker samples, typically with thickness more than 2 mm, machining may be performed to reduce the test thickness or adapt the specimen to the electrode configuration. When machining is necessary, the larger electrode, if electrodes of dissimilar sizes are used, is placed against the machined surface to ensure uniform stress distribution. Specimen thickness, a critical parameter in determining dielectric strength, is measured before and after the test with a precision of ±0.01 mm using ASTM D374 methods.

Specimens sensitive to environmental conditions such as moisture or temperature are measured and controlled before and during testing. The control of conditions ensures that the material is stable, thus eliminating variability caused by external factors. The conditioning process generally follows ASTM D618 guidelines, with specimens equilibrated at room temperature of 23 ± 2°C and 50 ± 5% relative humidity, unless otherwise specified. For materials, for which surface condensation may occur, wiping the specimen immediately before testing is necessary to minimize surface flashover risks. This step is crucial in stabilizing the specimen's dielectric properties under test conditions, providing reliable results.

Electrode configuration is critical in the testing procedure. Various electrode types are specified, with their selection dependent on the geometry and application of the material. Electrodes are typically made of brass or stainless steel, with polished surfaces to ensure full contact with the specimen and minimize surface irregularities that might affect the test. The test

medium further influences the results, as the sample may be tested in air or immersed in an insulating liquid, such as transformer oil conforming to ASTM D3487. Transformer oil, with a minimum breakdown voltage of 26 kV/mm of liquid, is commonly used to reduce surface discharges and flashover risks, particularly for thin specimens or high voltage tests.

The testing process involves applying alternating current (AC) voltage at power frequency, usually 50 Hz for Europe and 60 Hz for US. The voltage gradually increases until dielectric breakdown occurs, defining the point where the specimen can no longer insulate, resulting in an electrical discharge. The standard provides three methods for applying voltage, each suited to specific testing needs. The short-time test involves a continuous and rapid voltage increase, typically at rates of 500 V/s, although rates from 100 V/s to 5000 V/s are permitted. This method aims to induce breakdown in a time period within 10 to 20 seconds. The step-by-step test requires the voltage increase to be done in discrete steps, holding each step for a duration of 60 ± 5 seconds. Alternatively, durations of 20 ± 3 seconds or 300 ± 10 seconds can be used. Breakdown generally occurs within 4 to 10 steps, with the maximum voltage sustained at the last completed step, before breakdown, as the dielectric withstand voltage. Lastly, the slow rate-of-rise test requires that the voltage increase is done at a steady, slow pace, often between 1 and 100 V/s. This method is ideal for precise comparisons and ensures a breakdown at least 1.5 times of the starting voltage and within 120 seconds.

Upon breakdown, the results are meticulously recorded. These include the dielectric breakdown voltage in kilovolts (kV), the dielectric strength in kilovolts per millimeter (kV/mm), and observations regarding the location and nature of failure, such as edge flashover or partial discharge. For reliability, five tests are typically conducted for each sample, with the average values and standard deviations reported. Variability in results, often ranging from 1% to 20%, is accounted for through careful control of testing conditions and specimen preparation [6].

Oversheath

Measurement of thickness of the oversheath: Described in clause 10.6.3 of IEC 60229 [7], this test ensures that the oversheath meets the minimum thickness requirements described in (1).

$$t_{min} \geq 0.85 \cdot t_n - 0.1 \quad (1)$$

where t_n is the nominal thickness, and t_{min} is the minimum measured thickness.

2.3 Routine Tests

The solid insulation of a HV cable, during or after production can be tested using various tests, to ensure that the produced cables are up to quality standards for different aspects and characteristics of the insulation material. These tests are usually designed to not be destructive tests, unlike most of the type tests used to verify the power cable's design. The typical routine tests include:

Partial Discharge Test: To perform a partial discharge test, the necessary equipment is a robust power supply, a high voltage meter, a measurement circuit and a calibration device. All these components should be properly calibrated in order to detect and measure low power electrical signals. The power supply is expected to be a sine wave with frequency of 49 to 61 Hertz. The peak voltage should not be more than approximately 1.4 times the root mean square voltage with a tolerance of seven percent. While the power supply frequency does not disturb the calibration and the attenuation processes, the ordinary dielectric partial discharge characteristics of cable can theoretically be affected by it. So, this possibility should be considered in the measuring procedure, and so the test voltage should reach 1.75 times the nominal and stay at this level for 10 second and then reduce with small steps to 1.5 times the rated voltage as declared in Table 2 column 5. At this point there should not be any detected discharges larger than the declared one [3], [8].

Voltage Test: An alternating voltage of 2.5 U_0 (see Table 2 column 4), applied between the conductor and the metal sheath, should be set gradually and held at this level for 30 minutes, the insulation should not observe any breakdown of the insulation after testing [3].

Table 2. Rated voltages per test [3].

1	2	3	4[a]	5[a]	6[a]	7[a]	8[a]	9[a]	10[b]
Rated voltage U	**Highest voltage U_m**	**Value of U_0**	**Voltage test of 9.3**	**Partial discharge test of 9.2 & 12.4.4**	**Tan δ test of 12.4.5**	**Heating cycle voltage test of 12.4.6**	**Lightning impulse voltage test of 10.12, 12.4.7 & 13.2.5**	**Voltage test of 12.4.7**	**Voltage test after installation of 16.3**
kV	kV	kV	kV	kV	kV	kV	kV	kV	kV
45 to 47	52	26	65	39	26	52	250	65	52
60 to 69	72,5	36	90	54	36	72	325	90	72

110 to 115	123	64	160	96	64	128	550	160	128
132 to 138	145	76	190	114	76	152	650	190	132
150 to 161	170	87	218	131	87	174	750	218	150

Oversheath

DC Voltage Tests: The oversheath should withstand, without any breakdown, a negative polarity d.c. voltage of 8 kV/mm per the nominal thickness of the oversheath, with the maximum applied voltage being up to 25 kV independent to the oversheath thickness [7].

Spark Test: The procedure of this test is described in IEC 62230 and in order to test the oversheath a metallic conductor should be passed through the jacket of the cable, with length bigger or equal to the length of the tested sheath and they should be in touch for the whole duration of the test. After the preparation stage the metallic conductor should be earthed for the a.c. test or connected to the negative pole of the d.c. voltage power supply. The voltage applied to the metallic conductor is between 6 kV/mm and 9 kV/mm of oversheath thickness with the maximum test voltage being between 15 kV and 25 kV for a.c. and d.c. voltage respectively [9].

2.4 Special Tests

Special tests are commissioned only when a cable is expected to face service conditions that lie outside the envelope verified by ordinary type and routine tests. Type tests are, usually, one-off design validations carried out under controlled electrical and thermal stresses, in juxtaposition to routine tests, which are factory-floor checks that confirm workmanship on every production length; neither regime asks, for example, whether a cross-linked polymer will creep under sustained tensile load at emergency temperatures, whether an oversheath will abrade against rocky back-fill, or whether galvanic attack will perforate a bonded metallic screen in a coastal trench. For those “exceptional-but-credible” scenarios the standards prescribe special tests such as the hot-set (IEC 60811-507) to assess high-temperature mechanical stability, the abrasion test (IEC 60840) for surface wear, the corrosion test (IEC 60229) for chemical resilience, and the air-oven ageing treatment (IEC 60811-401) to estimate long-term property drift. Because these trials purposely

drive the specimen to, or even beyond, worst-case limits, they are applied only (i) during initial qualification, if the installation environment demands proof of extra robustness, (ii) after any substantive change of compound, layer thickness or supplier that could alter non-electrical properties, or (iii) in forensic or audit campaigns, when field performance has been poorer than expected. In short, special tests bridge the reliability gap left by the standard programs: they translate “pass” on a laboratory voltage withstand into confidence that the same cable will also endure sustained heat, mechanical abuse and chemical exposure over decades of real-world operation [3], [7], [10], [11].

CHAPTER 3: EXPERIMENTAL SETUP

3.1 Introduction

To investigate the dielectric properties of high voltage cable oversheath under lightning transient conditions, the cables were subjected to standardized impulse voltage testing. This setup comprises of a container filled with transformer oil, a 5-stage Marx generator, and the cable under test itself. A detailed analysis of the setup components is presented in this Chapter.

3.2 Container

The manufacturing procedure of the test tank emerged through four successive prototypes, which were evaluated using impulse conditions. For the needs of the test setup, a transparent vessel made from 5 mm thick plexiglass, with internal dimensions 400 mm × 400 mm × 200 mm, designed to provide ample clearance for a cable sample, while maintaining an oil level above the terminations. The tank was manufactured using plexiglass pieces which were glued using epoxy glue. This welding produced optically clear seams and a preliminary check, filling the tank with water, showed no visible weeping at the welding spots.

After the epoxy had cured for twenty-four hours, the container was filled with naphthenic insulating oil using a hand-operated piston pump (Figure 8). The insulating oil has a nominal breakdown voltage ≥ 75 kV (2.5 mm, per IEC 60156 [12]). The relevant oil characteristics, as taken from the datasheet, are tabulated in Table 3.

During the twentieth impulse voltage test a dielectric failure occurred. The accompanying shock wave propagated through the liquid and concentrated on the two vertical corner seams. Both seams fractured along their entire length and the acrylic box emptied. Although no personnel was endangered, the event demonstrated that a single-wall acrylic structure offers insufficient mechanical redundancy for repetitive impulse work.


Figure 8. Oil filling with manual pump.

Table 3. Characteristics of insulating oil.

Properties	**Units**	**Methods**	**EKO Insulating Oil**
Density at 20°C	g/ml	ISO 12185	0.875
Viscosity at 40°C	cSt	ISO 3104	9.7
Viscosity at -30°C	cSt	ISO 3104	1092
Flash point (PMCC)	°C	ISO 2719	144
Pour Point	°C	ASTM D5950	-55
Water content	mg/kg	IEC 60814	8
Dielectric Dissipation Factor (DDF) at 90°C		IEC 60247	0.001
Breakdown voltage, before treatment, 2.5mm	kV	IEC 60156	57
Breakdown voltage, after treatment, 2.5mm	kV	IEC 60156	75

After the acrylic cube failed, it was selected to build an entirely new vessel with a free-standing triangular prism (Figure 9) rather than repair or recycle the damaged parts. Three fresh sheets of 8 mm UV-stabilised PMMA were cut in a CNC machine-cut with 60° bevels and solvent–

bonded on a jig that ensured a good apex alignment. The resulting prism (equilateral base 300 mm, height 500 mm) eliminated the long 90° corner seams, which were split in the first tank and presented a single broad face that could be backed externally by a plywood brace. Filling was performed indoors with a battery-driven screwdriver, rotary barrel pump, as shown in Figure 10. Although the prism's thicker walls withstood the static stress from the oil filling, the first full-energy flashover generated a streamer that drilled straight into the narrow apex; the concentrated shockwave fractured the apex bond resulting in destruction of test setup. The geometry was therefore deemed intrinsically too fragile for repetitive impulse voltage hits and was withdrawn after a single test.

Figure 9. Second setup: Triangular shaped vessel.

Figure 10. New oil filling process.

A third prototype sacrificed transparency in favor of impact resilience. A single food-grade polypropylene crate (600 mm × 400 mm × 300 mm, wall thickness 3 mm) was lined with a heavy-duty high-density polyethylene bag and filled inside the laboratory. After three impulses a breakdown event, created a pin-hole in the crate floor, demonstrating that a single polymer wall—although tougher than acrylic—could still be melted by an internal arc.

Experience from the first three failures converged in the final nested-container assembly (Figure 11). Two identical polypropylene crates are stacked, doubling the wall thickness and creating a 40 mm interspace that forms an internal buffer. The specimen is carried by a curved-side polypropylene saddle repurposed from a bushing transit package; the holder keeps the conductor axis at least 20 mm above the acrylic plate under all operating conditions.

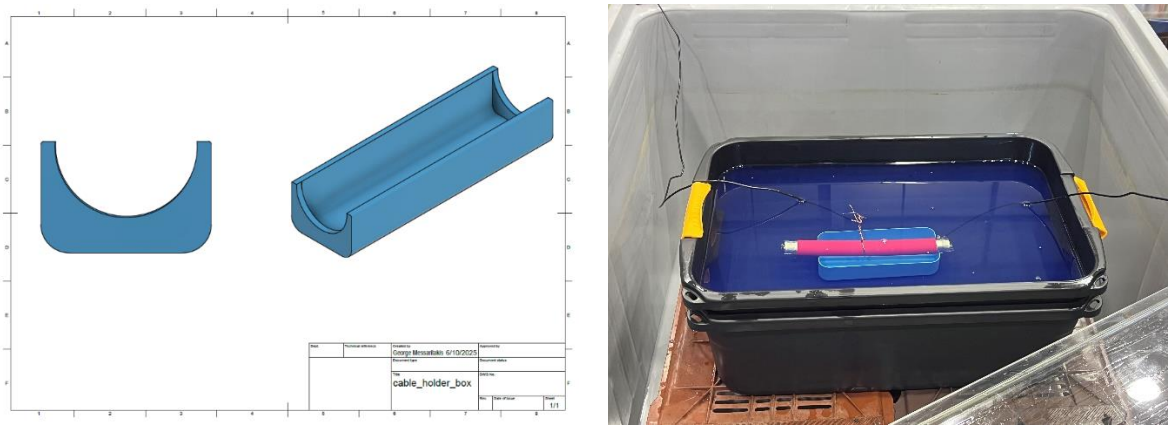

(a) (b)

Figure 11. The custom cable base (a) and the final container (b).

The entire stack is placed in a 1000ℓ high-density polypropylene intermediate bulk container that fulfils three roles simultaneously: tertiary containment, mechanical support and acts as a mobile trolley (Figure 12). Since this system was adopted for more than thirty voltage impulses with magnitude up to 450 kV, without any structural damage, the assembly satisfies all operational requirements: dielectric withstand, visual accessibility, ease for cleaning and, crucially, mechanical resilience under repetitive breakdown duty.

Figure 12. Outer protective box.

3.3 Marx generator

Marx generator is an impulse voltage multiplier circuit that charges capacitors in parallel and discharges them in series. For an n-stage generator, the output voltage V_{out} is given by (2).

$$V_{out} = n \cdot V_{charge} \quad (2)$$

where V_{charge} is the DC charging voltage per stage, for the purpose of this study a 5-stage Passoni-Villa Marx generator was used. The circuit of the Marx generator is depicted in Figure 13 exploits two physical phenomena; the capacitive voltage multiplication via series discharge and the spark-gap switching triggered by cascading overvoltage.

The Marx generator consists of various components, each fulfilling a specific task. Particularly it has:

- Charge capacitors
- Spark gaps
- Trigatron switch
- Charging resistors
- Front and tail resistors
- Capacitive divider

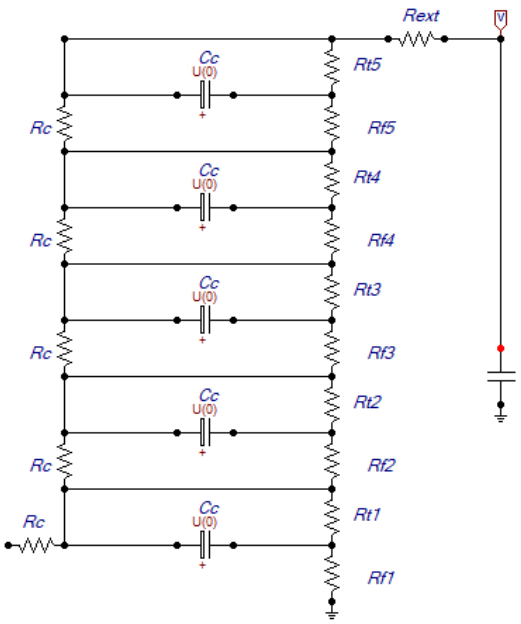

Figure 13. Circuit of a 5-stage Marx Generator.

Charge capacitors

Charge capacitors are responsible for providing output energy to the tested specimen. Passoni-Villa's generator used is equipped with 5 capacitors, that make up the generators capacitor bank. The capacitors' data label is shown in Figure 14. The label shows that each capacitor has a maximum charge level of 100kV and a capacitance of 0.5 μF, so the final total energy (E) that this Marx generator can provide is given using the equation (3).

$$E=\frac{1}{2}C_{total}V^2_{charge} \quad (3)$$

Where C_{total} is the total capacitance of the Marx generator. Using (3) and the nominal values of the capacitors, the total energy was calculated 12.5 kJ.

Figure 14. Charge capacitor data label.

Spark gaps:

Spark gaps are the critical switching elements in Marx generators, enabling the charged capacitors to be connected in series and deliver the voltage impulse on the device under test (DUT). Their function is both fundamental and irreplaceable. They provide electrical isolation during capacitor bank's charging, as they act as open circuits, due to their gap distance. The breakdown voltage of the gaps is larger than the charging voltage of the Marx generator. Afterwards the spark gaps are triggered and discharged at the same time, thus generating a large impulse voltage from all charged capacitors. To maintain the spark gaps in good shape and preserve their advantages they had to be cleaned from deposits and dirt using special paste and sandpaper. Before and after condition is shown in Figure 15.

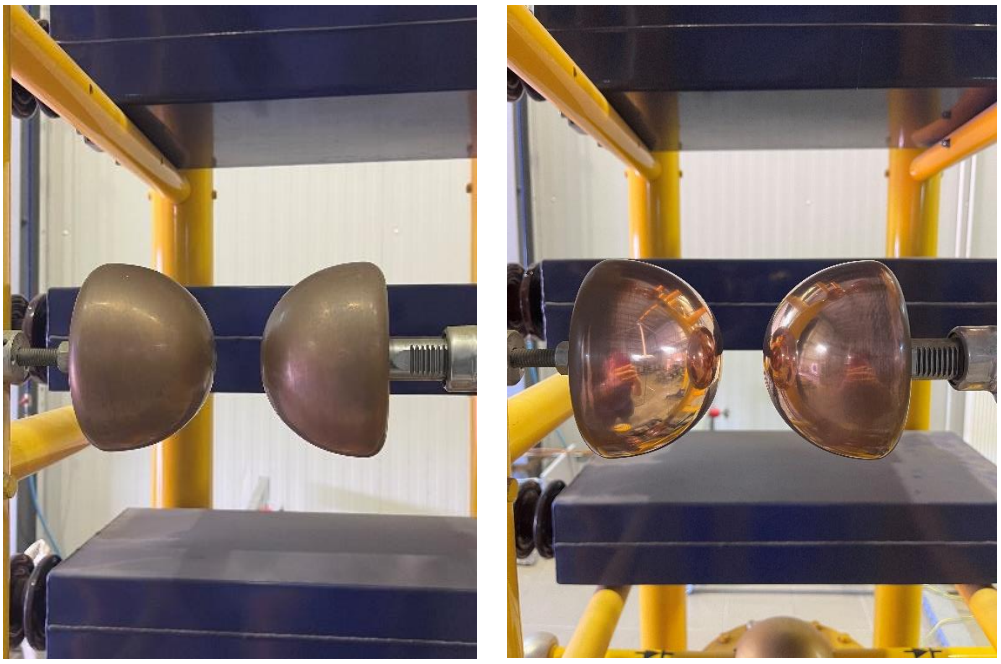

(a) (b)

Figure 15. Spark gap maintanance: Before (a) and after (b) cleaning.

Trigatron switch

When the capacitor bank is fully charged, meaning the capacitor bank is fully charged, the spark gaps should be triggered to create the voltage impulse. This trigger can either be uncontrolled or controlled. In the case of the Passoni Villa Marx generator, the triggering process is controlled via a trigger capacitor and a Trigatron switch. The trigatron's working mechanism is depicted in Figure 16.

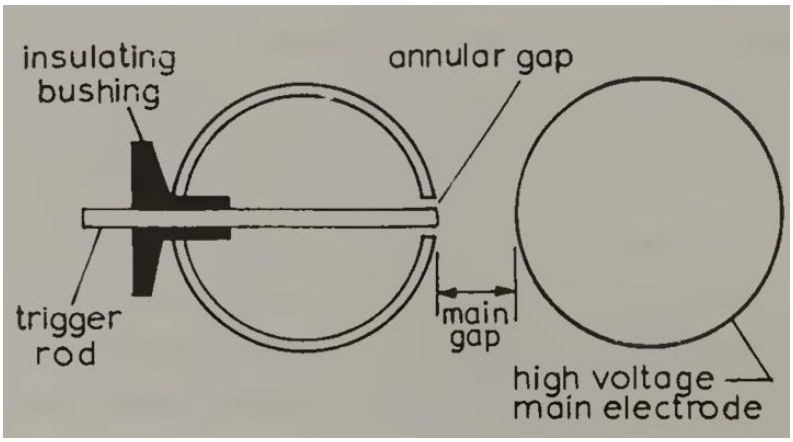

Figure 16. Trigatron trigger mechanism [13].

This mechanism is applied to the first spark gap pair, after the desired charge level is achieved, a trigger capacitor, which is connected directly to the trigger rod, is switched and creates a short pulse, thus creating the first spark. After that, the rest of the spark gaps are also triggered.

Charging resistors (R_c)

The charging resistors are used to charge the capacitor bank in a slow rate, so that they do not get strained. In this case, the generator consists of five charging resistors, each with a resistance of 3500 Ω. The position and the data label of the resistors are shown in Figure 17.

(a) (b)

Figure 17. Charge resistors' position (a) and data label (b).

Waveform-shaping components

After the capacitors discharge in series, the voltage waveform is shaped by a front resistor R_f with resistance of 12 Ω, a tail resistor R_t with resistance of 150 Ω, and a front capacitor C_2 with

capacitance of 4000 pF. This capacitor is also used as a capacitive divider and is depicted in Figure 19. In Figure 18 the front and tail resistors data labels are illustrated.

(a) (b)

Figure 18. Front (a) and tail (b) resistors data labels.

Capacitive divider

The previously discussed front capacitor installed at the output of the Marx generator, shown in Figure 19, performs two key functions. The first one is that it acts as the front capacitor: when the Marx stages discharge, their energy flows through a fixed front resistor into this relatively small external capacitance. Because its value is much lower than the capacitor bank's capacitance, it charges almost instantaneously and controls the steep rise of the lightning voltage impulse, thereby producing a waveform with the required 1.2 μs front time, while damping high-frequency oscillations and limiting post-breakdown voltage reversal.

Simultaneously, the same unit operates as an integrated capacitive divider. A second, much smaller capacitor located inside the housing is permanently connected in series with the main element and brought out to a low-voltage terminal. The pair forms a capacitive divider that scales the voltage to oscilloscope level without distorting its shape. Housing both limbs together ensures identical thermal conditions and minimises stray inductance, thus giving the divider an excellent ratio stability. By combining the two functions in one compact assembly, the topology eliminates extra wiring, reduces loop inductance and simplifies calibration, thereby ensuring that every voltage impulse delivered to the test object is both correctly shaped and accurately recorded.

(a) (b)

Figure 19. Capacitive divider placement (a) and data label (b).

3.4 Modification Procedure of the Marx Generator for Lower Impulses

After the first cable breakdown it was clear that the required voltage levels for cable testing would not exceed 100kV. However, when trying to achieve voltages lower than 60kV, the Marx generator did not produce correct waveforms and thus the generator had been modified per manufacturer's instructions, to a single stage impulse voltage generator. In order to achieve this, the charge capacitors had to be connected in parallel, and the rest of the components had to be rearranged.

The generator modification was a complex process with multiple steps. Initially, the generator was disassembled to access individual capacitor modules, charging resistors, and spark gap assemblies. Each spark gap was meticulously cleaned with abrasive paste and fine sandpaper to restore optimal switching performance. The primary modification involved rewiring the five capacitors and tail resistors, originally connected in series, into a parallel configuration. This rewiring required redesigning the internal wiring harness and installing parallel bus bars to guarantee equipotential voltage distribution across all capacitors. The internal arrangement was adjusted to accommodate this new wiring scheme efficiently, as shown in Figure 20.

(a) (b)

Figure 20. Copper bus bars for parallelizing capacitors(a) and modified generator with capacitors connected in parallel (b).

Each capacitor retained its individual charging resistor, which was repositioned to maintain independent charging paths. This step prevented undesired current sharing, ensuring uniform charging of each capacitor within the bank, as shown in Figure 21.

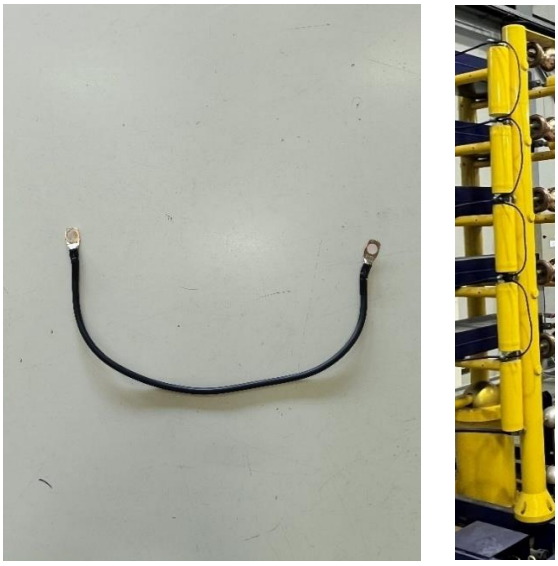

(a) (b)

Figure 21. Connection cable (a) attached to charge resistors (b).

According to the manufacturer, the tail resistors, which were originally distributed across individual stages, should be removed from their initial positions and should be reconnected as a parallel network downstream in the discharge circuit. This parallelization effectively lowers the overall tail resistance. The reduced tail resistance preserves the desired tail time—approximately 50 μs—ensuring the voltage decay of the impulse remains within IEC 60060-1 specifications. Simultaneously, the front resistors, which shape the front time of the impulse waveform, were readjusted in the new configuration. As the equivalent capacitance increased with the parallel connection of capacitors, the front resistor values were modified, to maintain the targeted front time near 1.2 μs, as shown in Figure 22 [5].

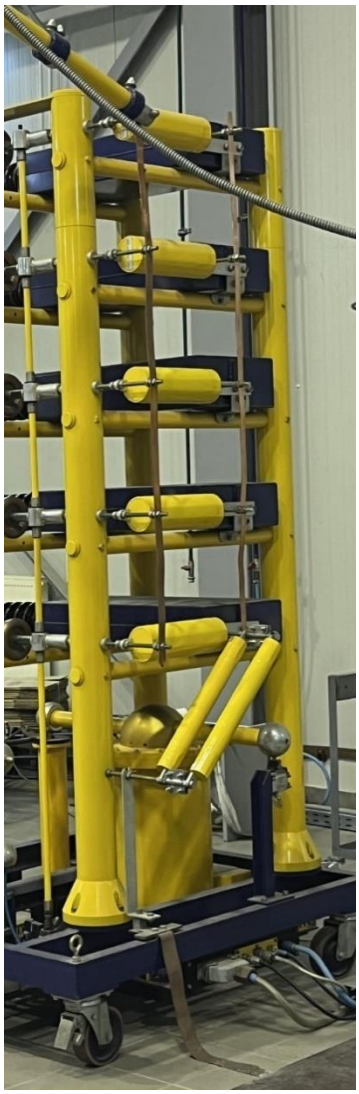

Figure 22. Tail and front resistors repositioned.

The spark gaps were realigned to maintain proper isolation during the charging phase and to guarantee synchronous triggering upon discharge. The trigatron and trigger capacitor systems were adjusted to ensure simultaneous firing across all parallel branches, a critical factor for stable and coherent impulse generation.

Given the anticipated increase in discharge current and altered internal wiring, the mechanical supports, insulation barriers, and spacing were reviewed and reinforced. These structural enhancements were essential to safely withstand the elevated electromagnetic forces during impulse voltage generation.

Following reassembly, the modified single-stage generator underwent systematic testing. Low-voltage tests verified uniform charging and spark gap isolation. Trigger synchronization was validated before full-voltage impulse testing conducted. The generator operation at approximately 17.1 kV output is depicted in Figure 23.

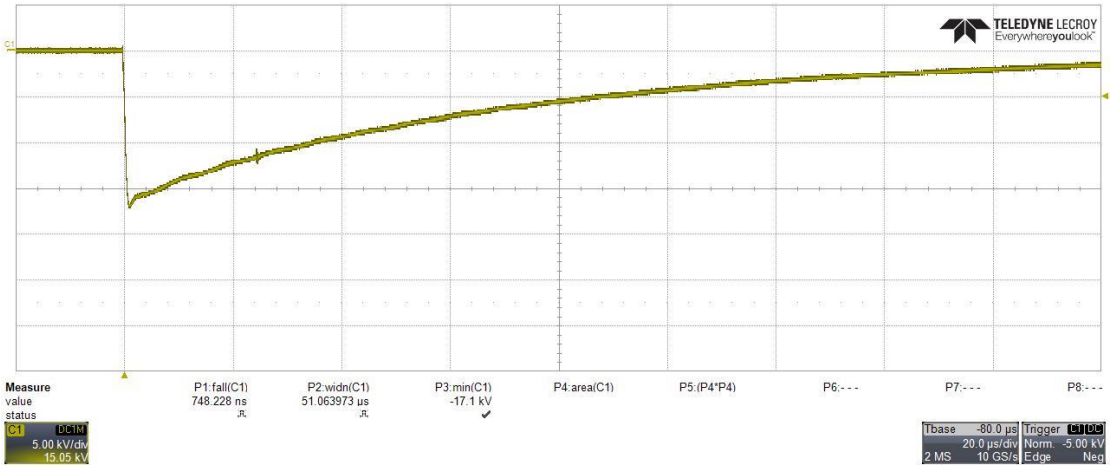

Figure 23. 17.1 kV voltage impulse with the single-stage impulse voltage generator.

Finally, the fully assembled and modified generator, installed in the laboratory environment is depicted in Figure 24. The finalized circuit is depicted in Figure 25.

Figure 24. Fully assembled single-stage voltage impulse generator.

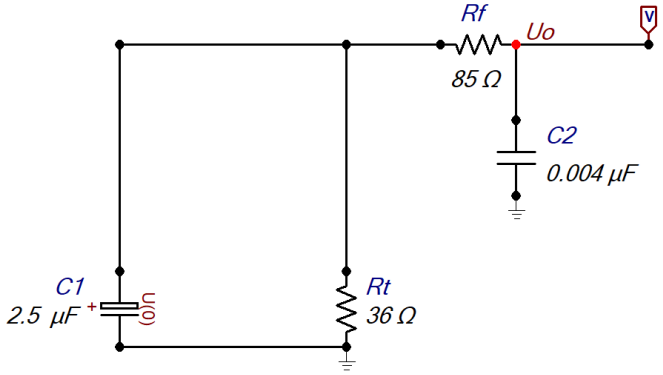

Figure 25. Single-stage impulse voltage generator circuit diagram.

3.5 Simulation of the Single-Stage Impulse Voltage Generator Using ATP-EMTP

To validate the performance and design parameters of the single-stage impulse voltage generator, a detailed simulation was conducted using ATP-EMTP software. The simulation

replicates the dynamic discharge behavior and output voltage waveform of the generator, configured as per the manufacturer's manual and previous theoretical calculations.

Simulation Setup and Methodology

The generator's equivalent circuit was modeled with the following key components:

- Charging resistor: R_c=3500 Ω.
- Capacitor bank: C_1=2.5 μF (Five parallel 0.5 μF capacitors).
- Front capacitor: C_2 = 4 nF.
- Wave-shaping resistors: R_f=85 Ω and R_t=36 Ω.

The circuit schematic (Figure 24) incorporates these elements along with measurement points to record the output voltage U_0. The transient simulation was executed to generate the voltage impulse waveform at the output node following the Marx generator triggering event.

Simulation Results

The post-processed results yielded the following key parameters:

- Front time, T_1 = 1.03 μs
- Tail time, T_2 = 64.73 μs
- Utilisation efficiency, η=97.7%

The utilization efficiency is a parameter that correlates the charging voltage U_{charge} to the peak impulse voltage U_{peak} and is calculated using (4).

$$\eta = \frac{U_{peak}}{U_{charge}} \quad (4)$$

The output simulated voltage waveform, in Figure 26, clearly demonstrates the characteristic double-exponential shape of a lightning impulse: a rapid rise to the peak voltage close to 100 kV, using the maximum charging voltage of 100 kV of the lab generator, followed by an exponential decay consistent with the tail time constant.

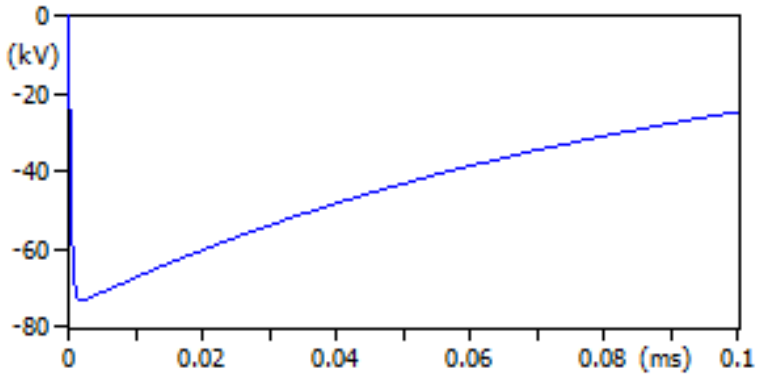

Figure 26. Simulated impulse voltage of the single-stage impulse voltage generator.

3.6 Comparative Analysis – Measured and Simulated Waveforms

A comparison between the simulation and theoretical results reveals close agreement with some expected differences:

Table 4. Theoretical vs Simulation

Parameter	**Measured Value**	**Simulated Value**	**Percentage Difference**
Front time T_1 [μs]	0.96	1.03	7.6%
Tail time T_2 [μs]	49.87	64.73	25.9%

The front time shows agreement, with only a 7.6% increase in the simulation. The tail time from the simulation is approximately 25.9% longer than the measured waveform. This discrepancy can arise due to factors not accounted for in the simplified simulated model.

- Parasitic inductances and stray capacitances in the physical circuit.
- Gradual degradation of the generator components due to the electrical discharge.

Despite this, the simulated front time still lies within practical limits for many testing applications, and the overall impulse waveform remains a valid representation of the target 1.2/50 μs lightning voltage impulse.

3.7 Cables Under Test

Cable Description — N2XS(F)2Y 1 × 300 RM 110 kV (DIN VDE 0276-620)

This cable is a single-core, 110 kV-rated power cable intended for high-capacity underground transmission in Central-European utility networks. The cable is depicted in Figure 27. Its principal layers, listed from the conductor outward, are summarised below:

- Conductor — Cu 1 × 300 mm² RM: Compacted copper round-sector conductor (IEC 60228 Class 2 [14]).
- Inner semi-conductive screen: Extruded compound that equalises the electric field at the conductor/insulation interface.
- Insulation — XLPE: Cross-linked polyethylene providing the primary dielectric barrier, high breakdown strength and excellent thermal-ageing performance.
- Outer semi-conductive screen: Bonded layer ensuring a smooth equipotential surface and remaining intact during oversheath tests.
- Metallic sheath: Helically applied annealed-copper wires with counter-spiral copper tape, offering a low-impedance fault-current path and radial electric-field shielding.
- Longitudinal water-blocking layer “F”: Swellable copper-laminated foil plus water-blocking tape that prevents moisture migration along the core should the jacket be damaged.
- Oversheath — Black carbon loaded layer: Robust oversheath that resists mechanical and electrical stresses.

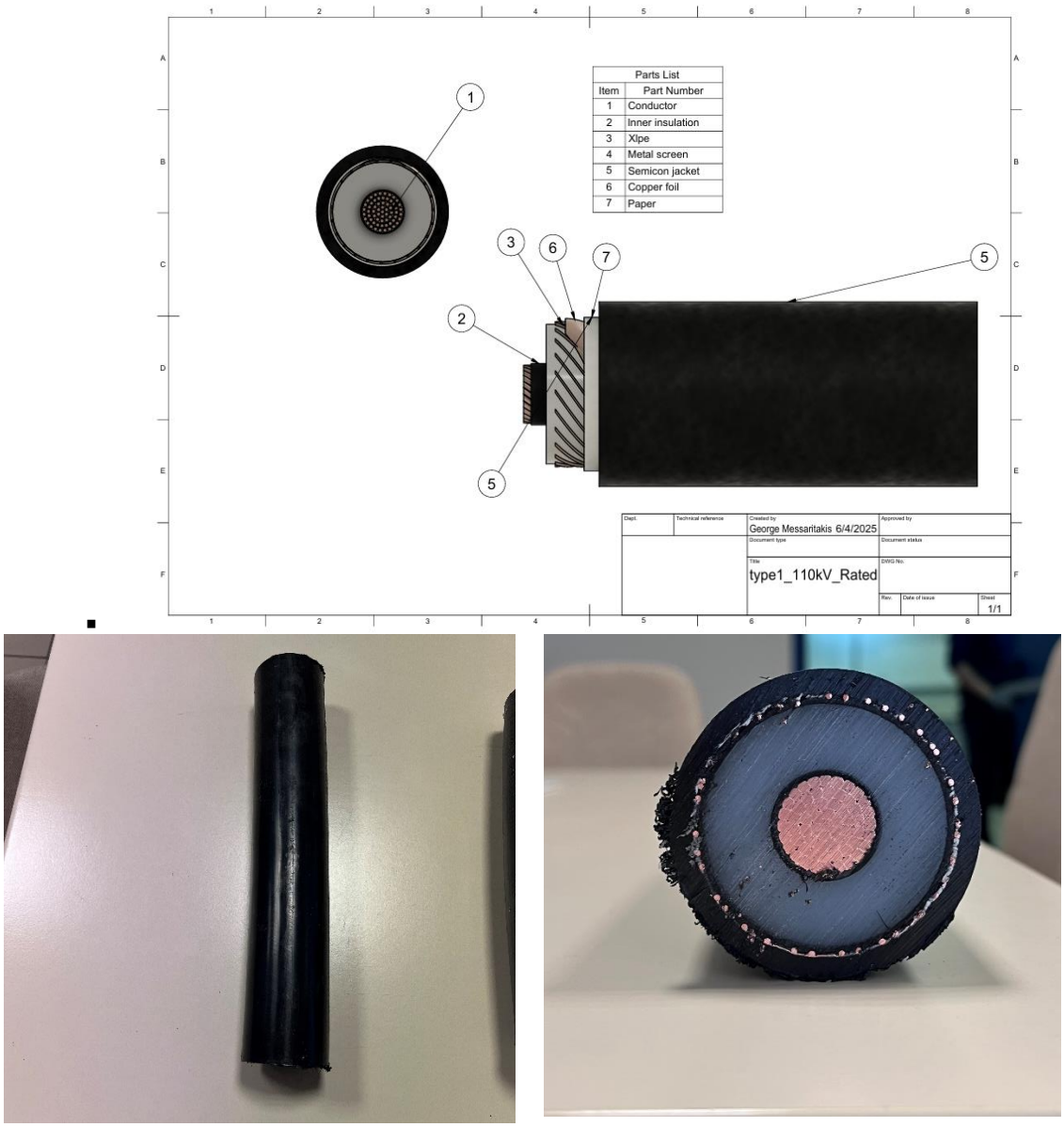

Figure 27. N2XS(F)2Y 1 × 300 RM 110 kV cable.

Cables of this construction are routinely deployed in urban areas, GIS-substation exit circuits and industrial interconnections where underground installation is mandatory. The copper wire screen delivers high short-circuit capability, while the longitudinal water-blocking system safeguards performance in wet soils or flooded ducts. The XLPE insulation permits thermally efficient operation at conductor temperatures up to 90 °C under steady load. The rugged HDPE oversheath withstands direct burial, tunnel installation and water-cooled conduit environments, and the factory-applied outer semicon expedites post-lay tests by enabling DC-sheath and impulse-sheath withstand checks without additional surface treatments. These features collectively make

the cable a preferred choice for reliable, high-power transmission in space-constrained or environmentally sensitive corridors.

Installation of oversheath impulse testing rings on cable ends

To expose the underlying copper sheath to install rind and testing leads on one end of the specimens, the factory-applied graphite jacket was removed mechanically with basic hand tools. The entire operation takes three to five minutes per cable end and avoids heat or rotary cutters that might drive graphite particles into the polyethylene. A 35 cm cable section is secured horizontally in an 80 mm bench vice (Figure 28), the jaws tightened only enough to grip the HDPE jacket without ovalising the core. A fine-tooth hacksaw is used to score a swallow 360° groove around the jacket at the prescribed strip line (Figure 28). The blade is kept square to the surface, and cutting ceases as soon as the bright spiral of copper wires becomes visible.

Figure 28. Saw and slicing procedure.

With the circumferential groove complete, the hacksaw is guided along the cable axis to open a single longitudinal slit from the score line to the sample end. This produces a tongue of jacket that can be lifted without nicking the copper screen. A flat-bladed screwdriver is then inserted into the slit and tapped gently with a raw-hide mallet (Figure 29); the soft face prevents impact damage to the insulation while the screwdriver acts as a wedge, gradually raising the graphite layer away from the HDPE.

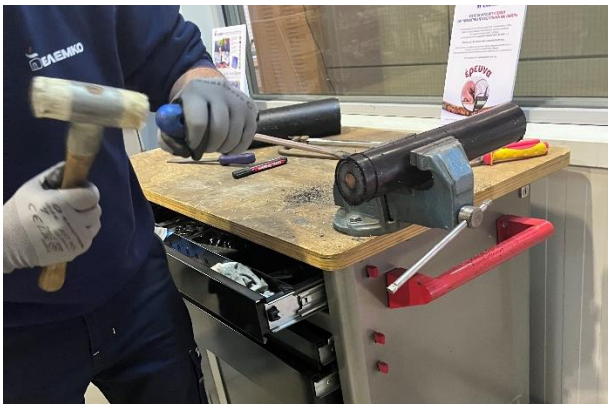

Figure 29. Jacket ring removal tools and procedure.

Once a sufficient flap has been freed, the jacket is peeled off in a smooth, circular motion (Figure 30). If resistance is felt, the longitudinal cut is extended in short increments rather than forcing the peel, thereby avoiding gouges in the copper screen. Residual graphite dust is wiped away with isopropyl-alcohol, leaving a clean oversheath surface ready for corona-ring installation and impulse-withstand testing.

Figure 30. Jacket ring.

Measuring the Oversheath Ring Thickness with a Vernier Caliper

Once the graphite-loaded jacket has been peeled away, a narrow band of the exposed HDPE oversheath. The band is cut with a fine saw while the cable remains in the bench-vice, ensuring that the cut faces are perpendicular to the cable axis and that the ring is not distorted. A digital vernier caliper (Figure 31) is zero-calibrated and used for thickness measurements. The ring is positioned lightly between the jaws so that the measurement axis is radial. Ten readings are taken at points roughly 36 degrees apart around the circumference, beginning with the thinnest visible

location and rotating the ring between successive measurements. Each value is recorded to the nearest 0.01 mm in the specimen log. With these measurements the arithmetic mean is calculated.

Figure 31. Vernier caliper for thickness measurement.

The measured ring is finally sealed in a labelled bag and attached to the test dossier, providing traceable physical evidence of the oversheath-thickness check. Care is taken throughout to handle the ring only with clean nitrile gloves and to keep the caliper jaws exactly parallel to the ring faces, thereby avoiding surface contamination and cosine-type measurement errors. The results of the measurements are shown in Table 5.

Table 5. Thickness measurements from 110kV cables.

HV Cable 110kV	AVG value [mm]
SPECIMEN 1	**3.892**
SPECIMEN 2	**3.905**

Cable Description — AL/XLPE/SWAS/PE 1 × 1200 RM 150 kV (IEC 60840)

This cable is a single-core, 150 kV-rated power cable intended for high-capacity underground transmission (Figure 32). Its principal layers, listed from the conductor outward, are summarised below:

- Conductor — AL 1 × 1200 mm² RM: Compacted round-sector aluminum conductor combining low resistance with reduced weight.

- Inner semi-conductive screen: Extruded compound that equalizes the electric field at the conductor/insulation interface.

- Insulation — XLPE: Cross-linked polyethylene (~ 18 mm thickness) providing the primary dielectric barrier, high breakdown strength and excellent thermal ageing performance.

- Outer semi-conductive screen: Bonded layer that maintains a smooth equipotential surface and remains intact during oversheath testing.

- SWAS — Seam-welded corrugated aluminum sheath: Longitudinally welded, helically corrugated Al tube offering a hermetic moisture barrier and a low-impedance metallic fault-current path while preserving flexibility.

- Bedding / water-blocking layer: Thin semi-conductive polymeric tape separating the metal sheath from the outer jacket, preventing galvanic interaction and equalizing surface potential.

- Oversheath — Black PE with thin outer semiconductive layer: Robust polyethylene jacket (~ 3.5 mm) that protects against mechanical and chemical attack; factory-coated with a graphite-loaded (~ 0.4 mm) semiconductive layer to facilitate on-site sheath-voltage and PD testing.

Cables of this type are routinely deployed in urban areas, substation interties and industrial supply lines where underground installation is mandatory. The aluminum SWAS provides a continuous radial moisture barrier—critical for extended wet corridors—while the XLPE insulation allows thermally efficient operation at conductor temperatures up to 90 °C under steady load. The rugged PE oversheath withstands direct burial, tunnel installation and the factory-applied outer semicon expedites post-lay testing by enabling DC-sheath and impulse-sheath withstand checks without additional surface treatments. These features collectively make the cable a preferred choice for reliable, high-power transmission in space-constrained or environmentally sensitive areas.

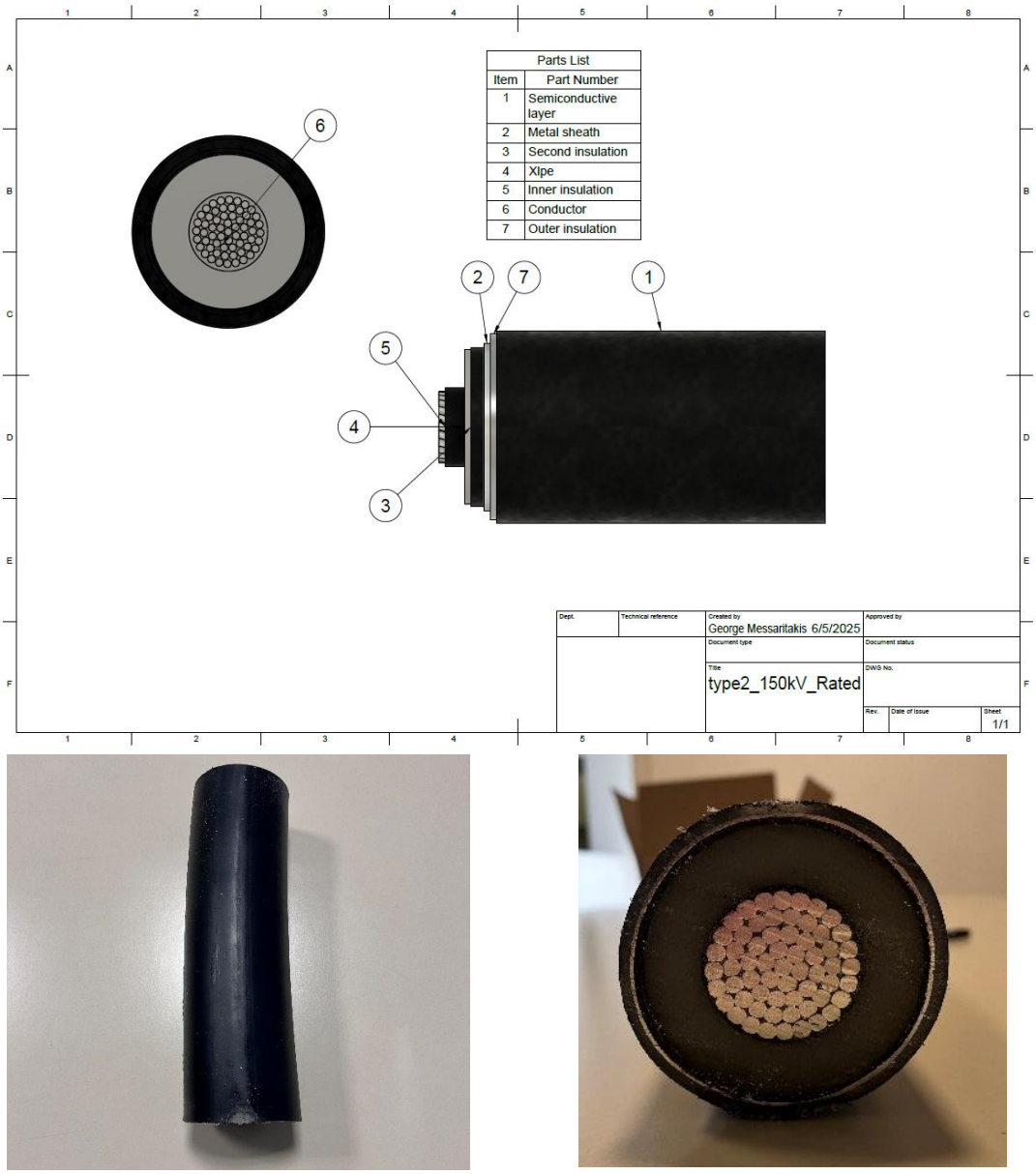

Figure 32. AL/XLPE/SWAS/PE 1 × 1200 RM 150 kV cable.

At this stage, only the outer polyethylene jacket was circumferentially slit and peeled away as a continuous ring, thereby exposing the underlying spiral-wound armour screen (SWAS) while leaving the semi-conductive outer layer and insulation entirely intact. Subsequently, ten jacket rings were excised, and each ring was gauged at ten equidistant circumferential positions with a calibrated vernier caliper; the readings for every ring were then averaged to obtain the representative jacket-thickness value for each of the ten specimens (Table 6).

Table 6. Thickness measurements for 150kV rated cable.

HV 150kV	AVG value [mm]
SPECIMEN 1	**3.59**
SPECIMEN 2	**3.79**
SPECIMEN 3	**3.65**
SPECIMEN 4	**3.67**
SPECIMEN 5	**3.54**
SPECIMEN 6	**3.61**
SPECIMEN 7	**3.73**
SPECIMEN 8	**3.7**
SPECIMEN 9	**3.55**
SPECIMEN 10	**3.81**

CHAPTER 4: SAMPLES PREPARATION AND EXPERIMENTAL PROCEDURE

4.1 Introduction

This chapter presents the experimental framework employed to assess the dielectric strength of two cable constructions under impulse-voltage stress. The methodology encompasses all the stages from the specimen selection and preparation through final analysis of the breakdown events. Although the cable types differ in geometry, materials, and screening arrangements, the testing workflow is organized into two parallel streams—one for the AL/XLPE/SWAS/PE 1 × 1200 RM, 150 kV design and the other for the N2XS(F)2Y 1 × 300 RM, 110 kV variant—while sharing common procedures for laboratory setup, oil-immersion environment, impulse-generator calibration, safety protocols, and data acquisition.

The objectives of this chapter are to document in rigorous detail the sequential actions undertaken for each cable type and to record the challenges encountered along with the mitigation strategies and procedural refinements that ensured reproducible, standards-compliant results. By presenting these topics in parallel, the influence of differences in conductor dimensions, semiconductive oversheath composition, and mechanical behavior under stress on handling and testing strategies becomes clear. Photographic illustrations and schematic diagrams are incorporated within the narrative to depict critical steps such as oversheath removal, specimen mounting, oil filling, impulse application, and post-test inspection.

The chapter begins with preparatory activities common to both cable types: selection and cutting of specimen lengths; verification of oversheath thickness against nominal requirements; fitting of terminations and corona rings; and calibration of the Marx generator to produce standardized impulse waveforms. Subsequent sections describe the specific preparation, installation, impulse application, and post-test evaluation routines for the 150 kV cable, followed by an equivalent account for the 110 kV cable. Post-test procedures and observations specific to each design are then discussed, accompanied by representative images and measurement records.

4.2 Experimental Procedure for Cable Type 2: N2XS(F)2Y 1 × 300 RM, 110 kV

Upon receipt of the cable specimens, the preparation process began by selecting a representative length of approximately 35 cm per sample, matching the dimensions used for other dielectric-strength tests. The specimen underwent careful stripping of its outer layers according to the methodology described in the preceding chapter. In particular, the tip region from which a jacket ring had been previously removed (as detailed earlier) was inspected to confirm that the jacket removal was clean and that the semiconducting screen and insulation interface remained intact. As seen in Figure 33, the stripped core, comprising concentric copper conductors and semiconductive screen layers, was then examined for irregularities in cross-sectional geometry.

Figure 33. Type 2 cable.

Fabrication and attachment of copper ring terminals followed. Two rings (Figure 34) were formed from strands of the cable's own conductor material, cut and twisted into circular loops that would serve as electrodes and control rings during impulse application. One copper ring was positioned at the mid-length of the specimen, ensuring that it encircled the conductor assembly without compressing the insulation. The second ring was placed near the end where the jacket had been removed, aligning with the location of the striped tip. Each ring was secured tightly against the outer semiconductive screen, using fine copper wire to ensure consistent electrical contact around the circumference. Care was taken to avoid nicking the underlying insulation (Figure 35); protective gloves and appropriate pliers were employed during these manipulations.

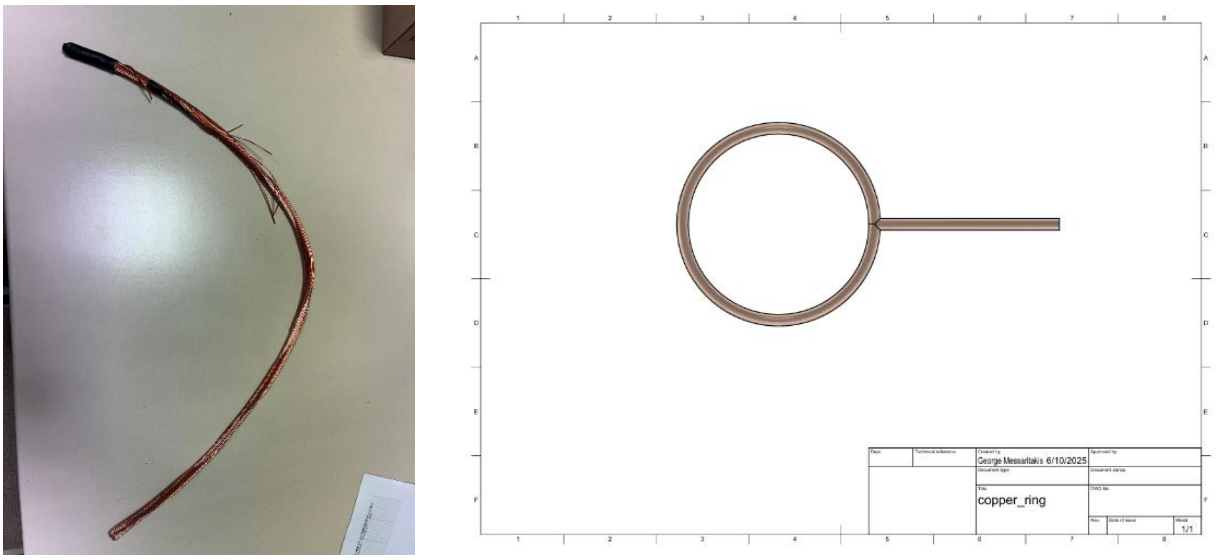

Figure 34. Copper ring.

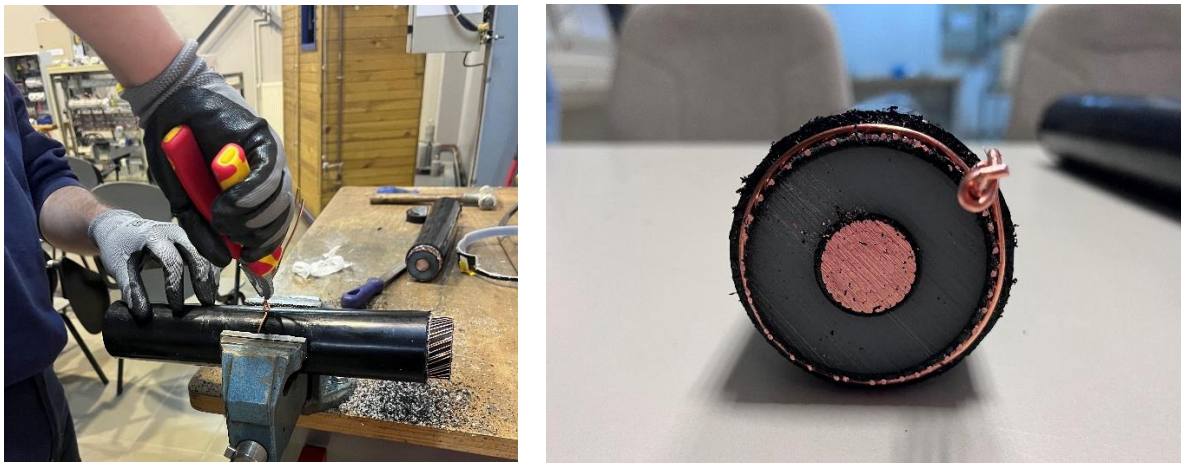

Figure 35. Copper ring attached to specimen.

With the rings in place, the specimen was ready for immersion in the oil-filled test container. The laboratory setup comprised a large insulated tank filled with transformer oil of known dielectric properties (naphthenic oil with antioxidant additives, breakdown voltage ≥75 kV per 2.5 mm), as seen in Figure 36. Prior experience had shown that proper filling and degassing of the oil are essential to minimize spurious discharges; thus, the oil level was allowed to settle and any visible bubbles were removed by gentle stirring and timed quiescence. The cable specimen, mounted on a non-conductive holder (Figure 36) within the container, was lowered so that its rings and central region were fully submerged, while the termination lead extended upward to connect to the impulse generator.

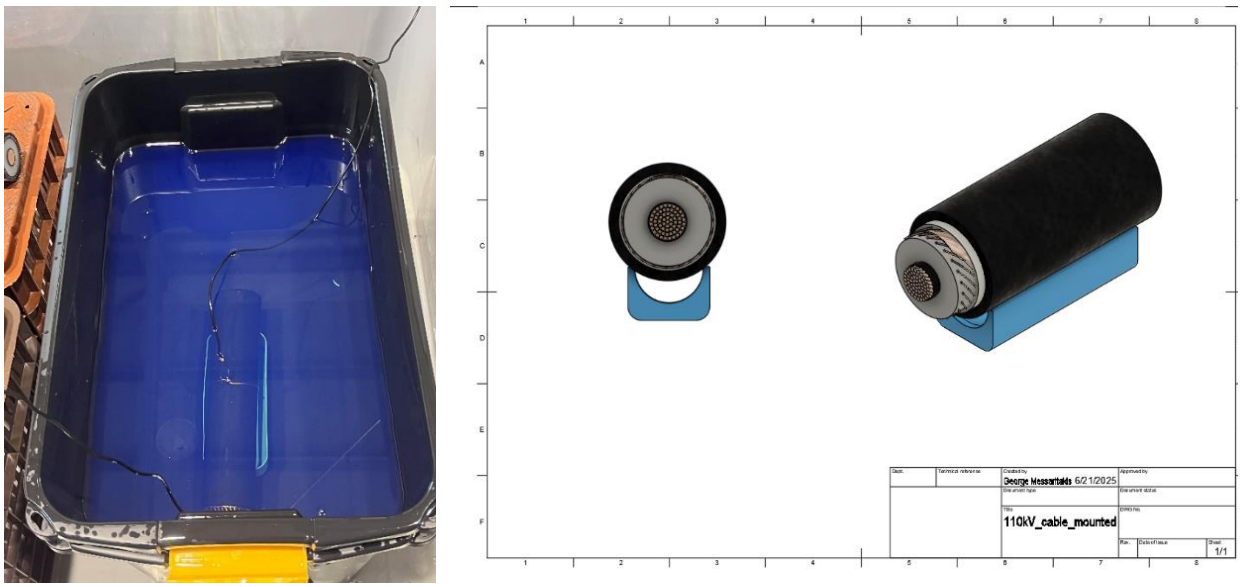

Figure 36. Specimen mounted on box.

During the first impulse application, the Marx generator was set to deliver a standard 1.2/50 μs lightning-impulse waveform at the nominal peak voltage expected for the 110 kV rating. However, the observed waveform exhibited a markedly faster decay (shorter tail) than the prescribed 50 μs decrement (Figure 37). Simultaneously, the characteristic noise of the impulse discharge suggested abnormal current pathways.

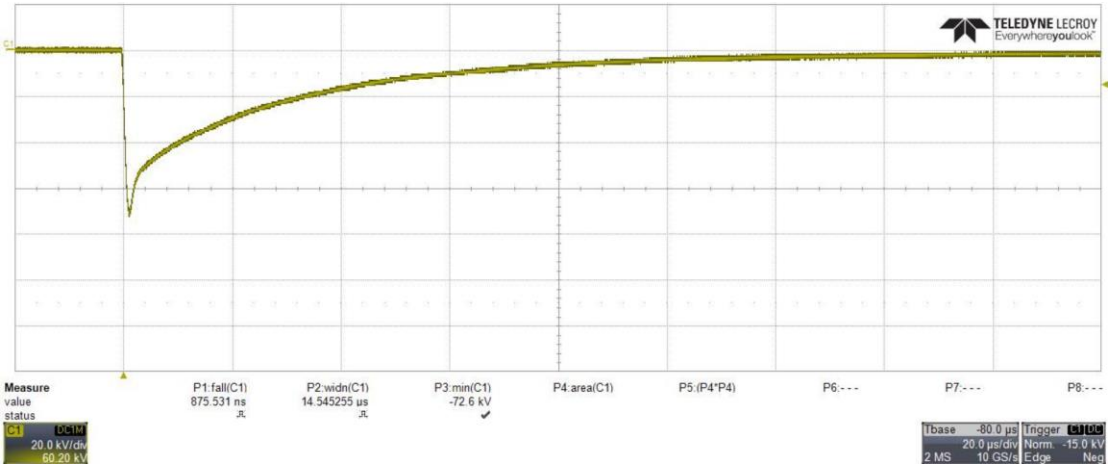

Figure 37. Distorted waveform.

To capture the discharge phenomenon visually, a long-exposure photograph was taken during an impulse shot. The camera sensor was set with a 4-second exposure to maximize the likelihood of recording any light emission in the oil tank. The resulting image revealed multiple luminous filaments emanating from the specimen region, indicating localized discharges. It was evidentiary, through visual inspection (camera photographs), that the discharge was not confined to the intended electrode gap but was escaping along the specimen surface, as seen in Figure 38.

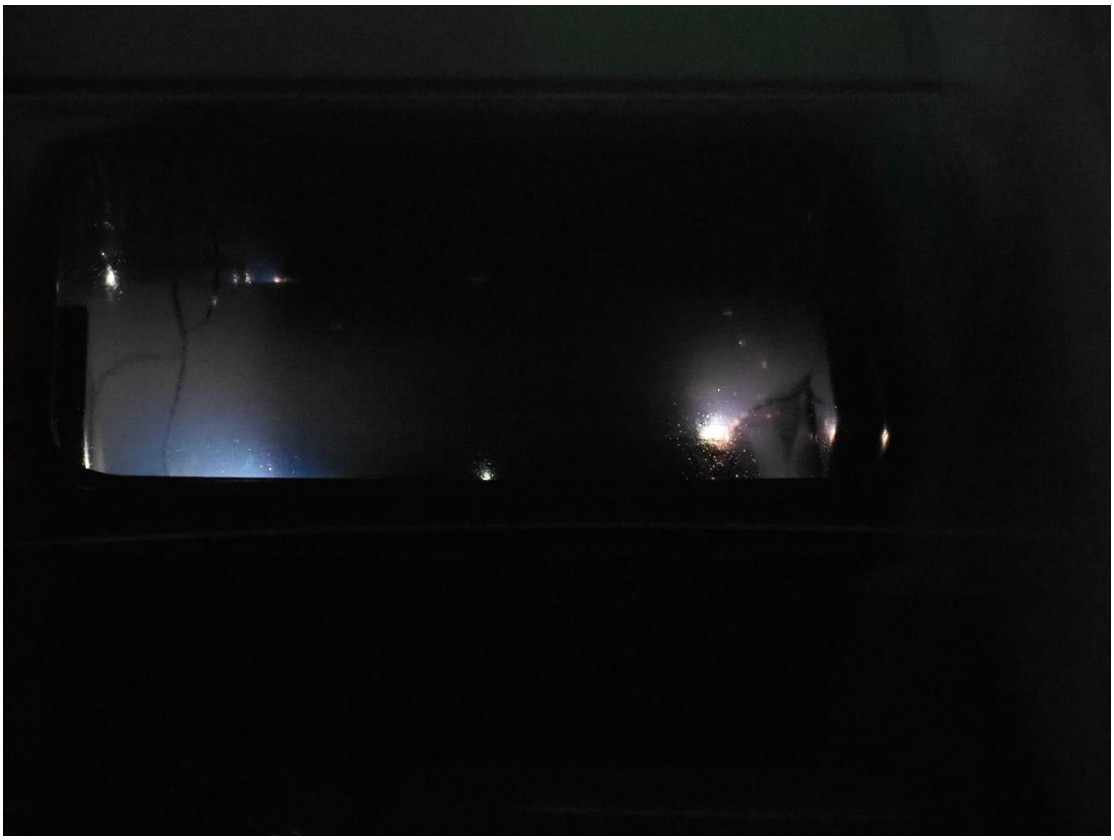

Figure 38. Creepage discharge long-exposure.

Prompted by these observations, what was hypothesized was that unintended resistance or current leakage paths were affecting the impulse waveform. One possibility considered was surface discharge between the semiconductive screen and the conductor core. To address this, an attempt was made to equalize potentials between screen and core. A metallic screw was inserted through the insulation near the mid-region (taking care not to damage the primary dielectric), and a short jumper cable was connected between this screw and the copper ring or core connection. The intention was to force the voltage gradient between screen and core to zero, in an effort to suppress the discharges along that interface.

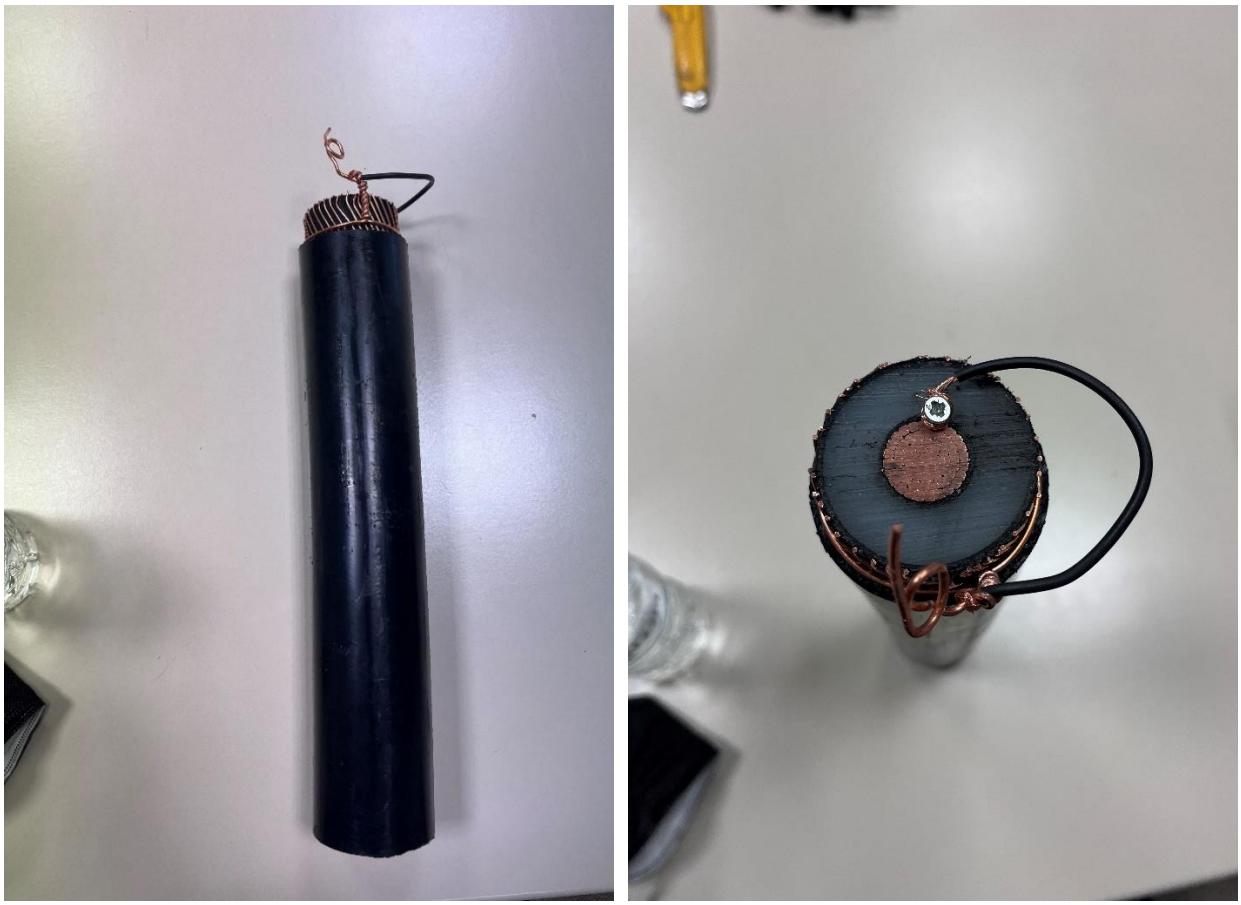

Figure 39. Potentials equalization modification.

Despite this intervention, subsequent impulse shots (Figure 37) still displayed the accelerated tail and audible signs of discharge. On inspection after the test, the specimen's surface exhibited burn marks and erosion consistent with surface (creepage) discharge. Photographs of the affected region revealed distinct channels of damage radiating from the copper ring toward the adjacent ends, confirming that the discharge had traversed the surface of the jacket material rather than occurring through the intended oil gap alone (Figure 40).

Figure 40. Cable after surface discharge.

The next step involved measuring the electrical resistance of the jacket between its exposed edges. Using a precision ohmmeter, the resistance was measured across the jacket thickness and along its surface over the 35 cm length. The reading of approximately 840 Ω (Figure 41) denoted that the external layer was mainly semiconductive; suggesting a conductive path along or within the jacket, which could readily promote surface discharge under high voltage not allowing dielectric strength measurements.

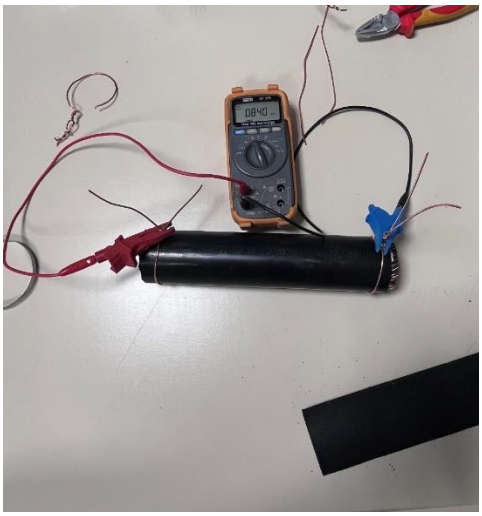

Figure 41. Cable's resistance.

In an attempt to restore a higher insulating resistance, the outer jacket surface was lightly abraded (Figure 42) using 80-grit sandpaper to remove any superficial conductive layer or contaminants. After sanding, the resistance was increased up to the level of 1500 Ω. Despite this

increase, further impulse shots still produced irregular waveforms and audible discharge events. The recorded waveforms continued to deviate from 1.2/50 μs, with abbreviated tail times and erratic oscillations.

Figure 42. Sanding specimen.

Figure 43. Resistance after sanding.

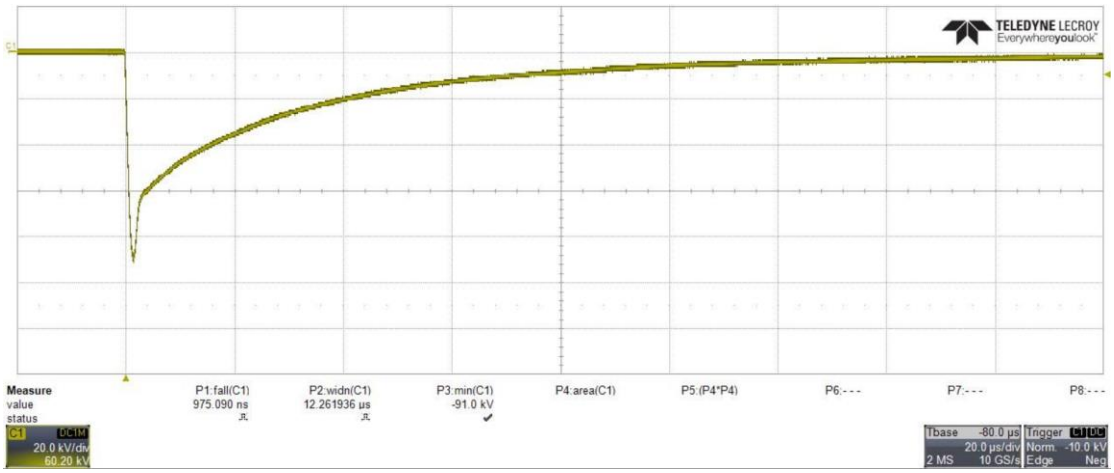

Figure 44. Waveform of sanded cable.

Faced with persistent surface discharge, it was concluded that the jacket material itself was inherently semiconductive throughout its thickness, not merely a thin surface layer. Consequently, the cable design precluded conventional impulse testing in oil, since the semiconductive jacket would always facilitate surface discharge under high stress (Figure 21).

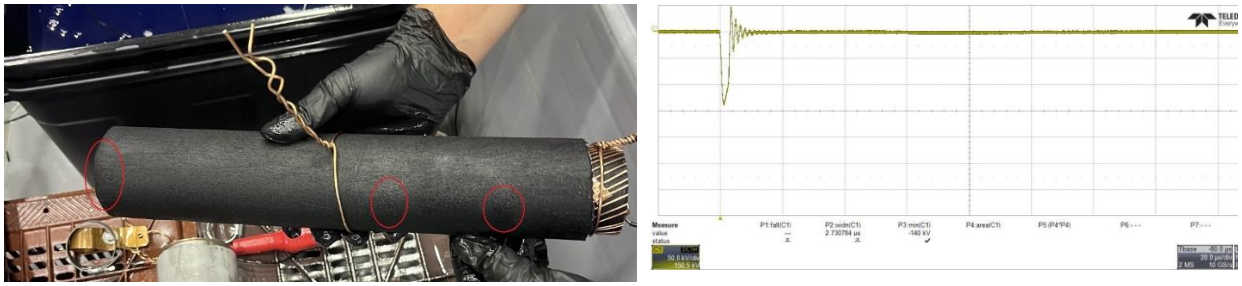

Figure 45. Surface discharge on scraped cable.

4.1 Experimental Procedure for Cable Type 1: AL/XLPE/SWAS/PE 1 × 1200 RM, 150 kV

The 150 kV cable specimen was prepared and tested under conditions intended to replicate service-relevant stresses, with careful attention to surface condition, electrode attachment, dielectric environment, and high-voltage impulse waveform fidelity. Initially, the outer jacket of the cable was stripped to expose the underlying layers (Figure 46). A circumferential ring of the outer covering was removed at one end, revealing the semiconductive screen beneath (Figure 45). Similarly, as per section 3.1, the presence of a substantial semiconductive layer was not yet fully realized.

Figure 46. 150kV specimen with jacket ring removed.

Two copper rings were used from stranded conductor material and affixed to the specimen: one positioned at mid-length to serve as a grading or reference electrode, and one at the stripped end to act as the high-voltage connection. These rings were formed to match the conductor diameter precisely and were secured by wrapping and mechanical fastening to ensure low-resistance contact, while avoiding damage to the insulation. The insulation surface between the rings remained covered by the original black jacket at this point. The specimen was immersed in transformer oil (Figure 48) to provide a uniform dielectric medium free of air gaps (Figure 47).

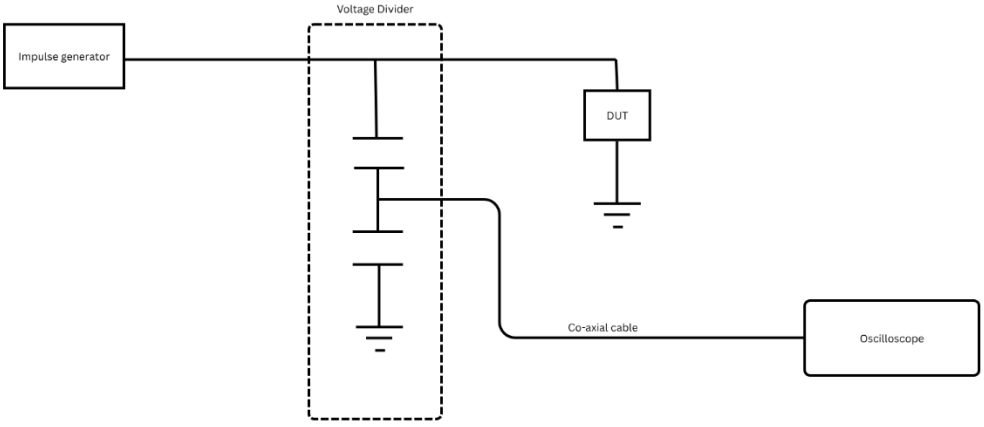

Figure 47. Equivalent test circuit.

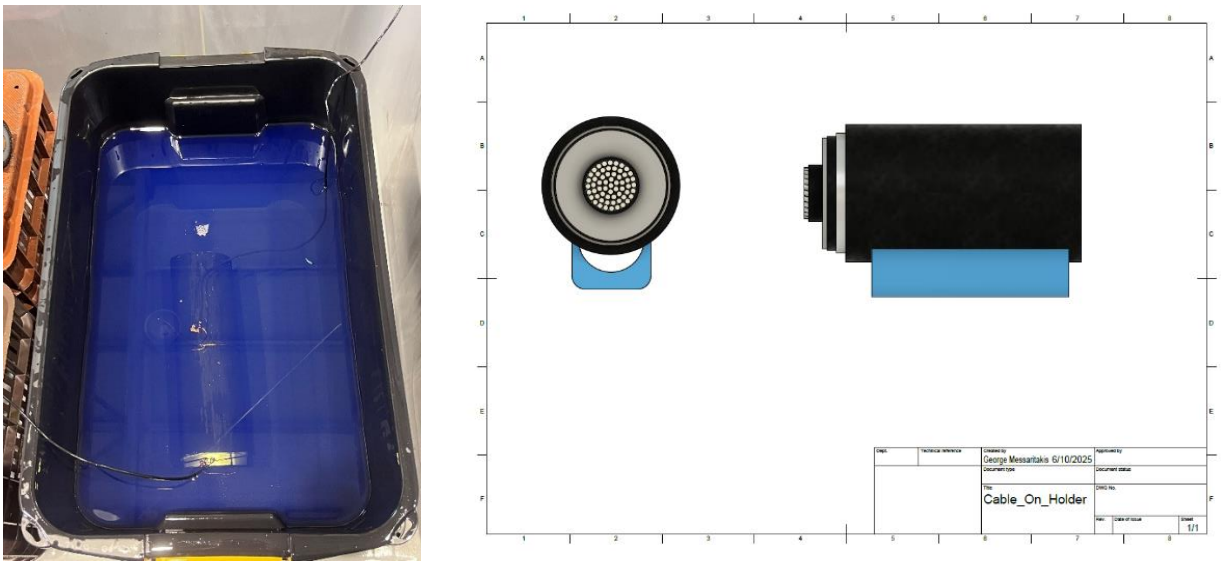

Figure 48. Specimen zero.

Upon the first application of lightning impulse voltage, the recorded waveform exceeded the expected 1.2/50 μs shape. The decay exhibited again an abnormally rapid tail, and the overall profile suggested a leakage path or surface discharge influencing the impulse behavior. An oscilloscope capture of this initial waveform (Figure 25) clearly showed the shortened tail time and nonideal decay characteristics.

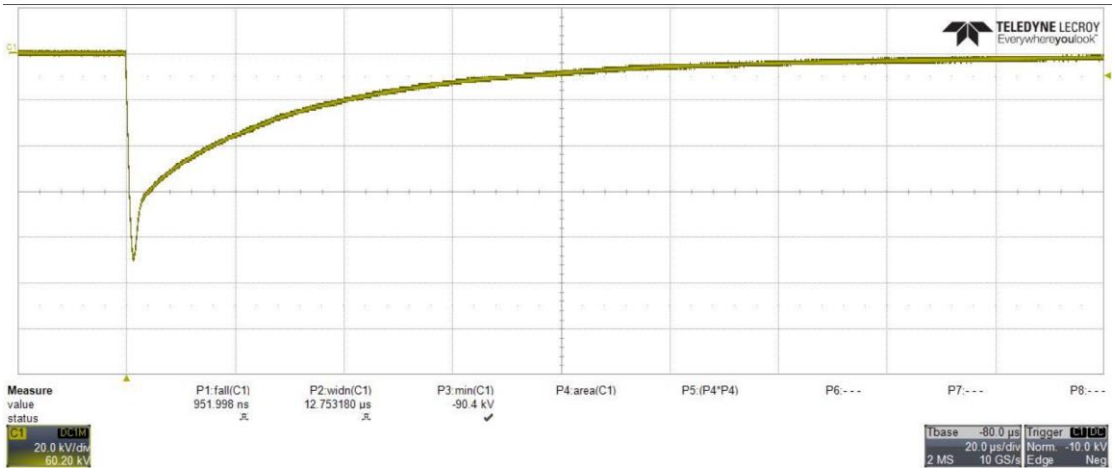

Figure 49. Output waveform from specimen zero.

Such distortion indicated that the specimen surface was conductive under high voltage rather than behaving as a purely insulating barrier. To investigate the cause, the surface resistance was measured between the mid-length ring and the end ring using a precision ohmmeter. The measured

resistance was in the order of a few KΩ for the 35 cm specimen, confirming a conductive or semiconductive path along the jacket surface (Figure 50).

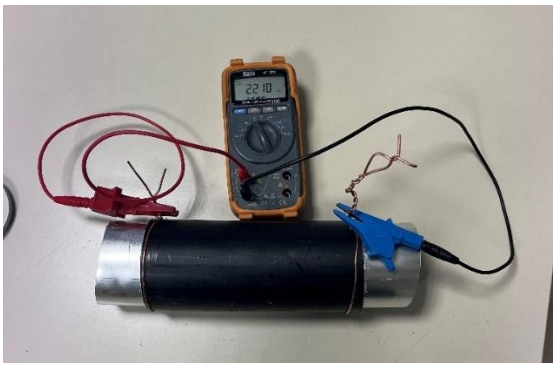

Figure 50. Resistance measurement for 150kV rated cable.

Visual inspection after the impulse revealed carbonization traces of the outer layer indicative of creepage discharge. Photographs taken immediately after the impulse showed carbonized traces and localized damage where surface currents had discharged, confirming that the semiconductive jacket had permitted leakage currents and partial breakdown under the applied stress (Figure 51).

Figure 51. Burned jacket of specimen zero.

Recognizing that the semiconductive layer extended through a significant thickness—approximately two millimeters—mechanical removal was undertaken. Initial abrasion with coarse sandpaper proved insufficient, as residual semiconductive material remained and surface resistance stayed too low for valid impulse testing. A rasping tool was employed to scrape away the entire semiconductive layer uniformly around the circumference, exposing the underlying insulating material. During this process, the specimen was securely clamped to prevent movement,

and care was taken to remove the layer evenly without nicking the insulation beneath. After rasping, the surface exhibited a consistent matte appearance, free of the black semiconductive film (Figure 52).

Figure 52. Removal of semiconductive layer and specimen preparation.

Following the semiconductive layer removal, the surface resistance measurement was repeated (Figure 53), where in the resistance was increased dramatically into the GΩ range, indicating that the exterior now behaved as a high-quality insulator. This change in surface resistivity confirmed that the semiconductive path had been properly removed. With the insulation surface restored to a nonconductive state, the specimen was reassembled for testing.

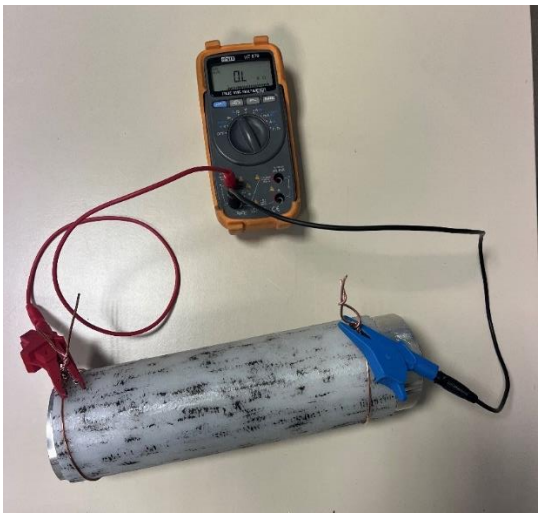

Figure 53. Resistance measurement without semicon layer.

A clean ring of insulation was cut at the opposite end using a fine-toothed saw, ensuring a perpendicular and smooth cut without frayed edges. New copper electrode rings were attached at the mid-length and stripped end, with careful wrapping of tinned copper braid to secure firm, low-

resistance contact without any remaining metallic screen elements. The assembly was rinsed in filtered oil to remove debris and then allowed to drain prior to immersion.

The prepared specimen was immersed in the oil container, with electrode connections routed through appropriate feedthroughs. Safety interlocks, monitoring equipment, and grounding references were checked in accordance with laboratory protocols. Impulse testing took place at a starting voltage of 45 kV 1.2/50 μs, incrementing in defined steps up to approximately 80–90 kV 1.2/50 μs. For each voltage level, seven impulse shots were applied, the oscilloscope was triggered to capture the waveform, and the data were exported as CSV files. The captured waveforms consistently displayed the correct 1.2/50 μs profile, with front time and tail time falling within the tolerance specified by relevant standards [5]. No abnormal tail shortening or distortion was observed, indicating that no surface discharge or leakage was present after removal of the semiconductive layer. Throughout the testing sequence, visual observation through the oil confirmed absence of creepage discharges along the insulation surface. After each shot, the specimen remained intact until the final puncture test at the highest voltage level. The puncture occurred cleanly through the insulation at the intended location, without lateral tracking or erratic flashover paths. Post-test inspection revealed the expected puncture marking point, with no carbonized tracks or surface creepage discharges

The experimental results with the 150 kV cable underscore the critical importance of assessing and, where necessary, removing semiconductive jacket materials when performing impulse testing. Without such removal, surface conduction can drastically distort impulse waveforms and lead to unreliable or invalid results. Following mechanical removal and verification of high surface resistance, the specimens exhibited the expected impulse behavior, confirming the integrity of the underlying insulation. This comprehensive procedure (Figure 54)—from initial stripping and electrode attachment, through diagnostic resistance measurements, mechanical layer removal, reassembly, oil immersion, stepped impulse application, data recording, and post-test inspection—ensured that the test outcomes accurately reflected the cable insulation's dielectric strength. The methodology and observations are presented in the figures and photographic records that accompany this thesis, illustrating each phase of the process and validating the final test results (Figure 55).

Figure 54. Examples of jacket insulation failures.

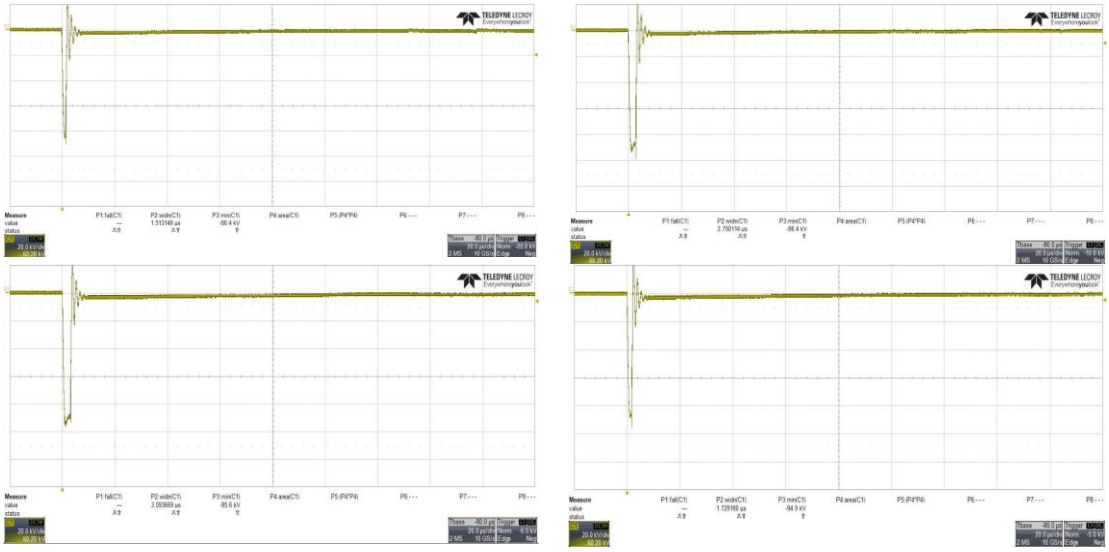

Figure 55. Breakdown waveforms for picked specimens.

CHAPTER 5: STATISTICAL ANALYSIS OF RESULTS

5.1 Introduction

In high voltage engineering, dielectric breakdown phenomena exhibit inherent uncertainty due to material variability, manufacturing processes, and testing conditions. Consequently, statistical methods are indispensable tools for quantifying and interpreting dielectric performance. This chapter provides an in-depth statistical analysis of experimental data collected during voltage impulse breakdown tests on high-voltage cable oversheaths. The analysis employs Weibull statistical distribution, justified by established prior knowledge from literature [15], [16].

5.2 Detailed Description and Preparation of Experimental Data

The experimental dataset comprises breakdown voltages from voltage impulse tests conducted according to IEC standards, employing a standard lightning voltage impulse waveform (1.2/50 μs). Specimens of various insulation thicknesses were tested to explore thickness-related effects. Each insulation thickness was meticulously measured using high-precision instruments (±0.01 mm accuracy), ensuring accurate characterization of the oversheath thickness, a parameter which is critical for interpreting the test results. Data preprocessing involved calculating breakdown probability, dielectric strength (kV/mm), facilitating direct comparison across specimens of different thicknesses, study of breakdown time related to breakdown voltage showing the withstanding of the jacket under high voltage stress.

5.3 Rationale for Statistical Methods Selection

Weibull Distribution

The Weibull distribution was selected based on its recognized suitability for modeling dielectric breakdown phenomena. It is particularly effective in modeling weakest-link behaviors common in insulation breakdown, where failure initiates at the most vulnerable microstructural defect. Liu et al. experimentally validated Weibull's applicability, demonstrating high accuracy for

low-probability events (e.g., 0.1% probability). Alternative distributions, such as normal or exponential, fail to capture the underlying breakdown mechanisms adequately, as they inherently assume symmetrical data behavior, incompatible with insulation breakdown physics [15], [16].

Coefficient of Determination (R^2)

The coefficient of determination (R^2) measures the proportion of total variance in experimental data explained by the chosen statistical model. This criterion was selected due to its intuitive interpretability, widespread acceptance in engineering regression analyses, and straightforward quantification of statistical distributions accuracy. When R^2 is close to unity indicates excellent alignment between empirical data and model predictions, confirming model robustness and reliability [15], [16].

5.4 Statistical Analysis Methodology

A structured statistical approach was meticulously followed:

- Data Extraction: Systematic extraction and validation of breakdown voltages from measurement records.
- Distribution Fitting: Application of Weibull distribution for the calculation of breakdown probability per impulse voltage level.
- Model Selection: Comparative regression analyses for correlation between breakdown voltage and oversheath thickness (linear, quadratic, exponential, and power-law) to determine optimal model via R^2 criteria.
- Result Interpretation: Calculation and detailed interpretation of Weibull parameters (α, β) and quantile voltages (U_{10}, U_{50}, U_{90}), along with the average electric field (kV/mm) required to break down the oversheath regardless of its thickness.

5.5 Detailed Analysis and Interpretation of Results

Breakdown probability via Weibull fitting

Figure 56 shows ten measured breakdown voltages plotted against the percentage of samples that have failed at or below each voltage. The horizontal axis runs from 79 kV to 89 kV in 1 kV steps, and the vertical axis from 5 % to 95 % in 10 % steps. Hollow circles mark the data points, and a dashed green line represents the fitted Weibull model, with a shape factor $\beta = 31.17$ and scale factor $\eta = 86.15$ kV, consistent with high exponents indicating narrow defect distributions as described by Hauschild & Mosch [15]. Vertical dashed guides mark $U_{10} = 80.2$ kV, $U_{50} = 85.1$ kV, and $U_{90} = 88.5$ kV, indicating the voltages at which 10 %, 50 %, and 90 % of samples have failed. Liu et al. reported similar Weibull slopes in XLPE films under impulse conditions, affirming the relevance of these quantiles for polymeric insulation. The close alignment of all points with the model line confirms that failure mechanisms are uniform across the sample set and that early, median, and late failures follow the same statistical pattern. From an application standpoint, the conservative design threshold U_{10} suggests that operating voltages should remain below 80.2 kV to limit failure risk to under 10 %, while U_{90} indicates that voltages up to 88.5 kV maintain 90 % risk of having a breakdown, supporting reliable cable performance under normal conditions [16].

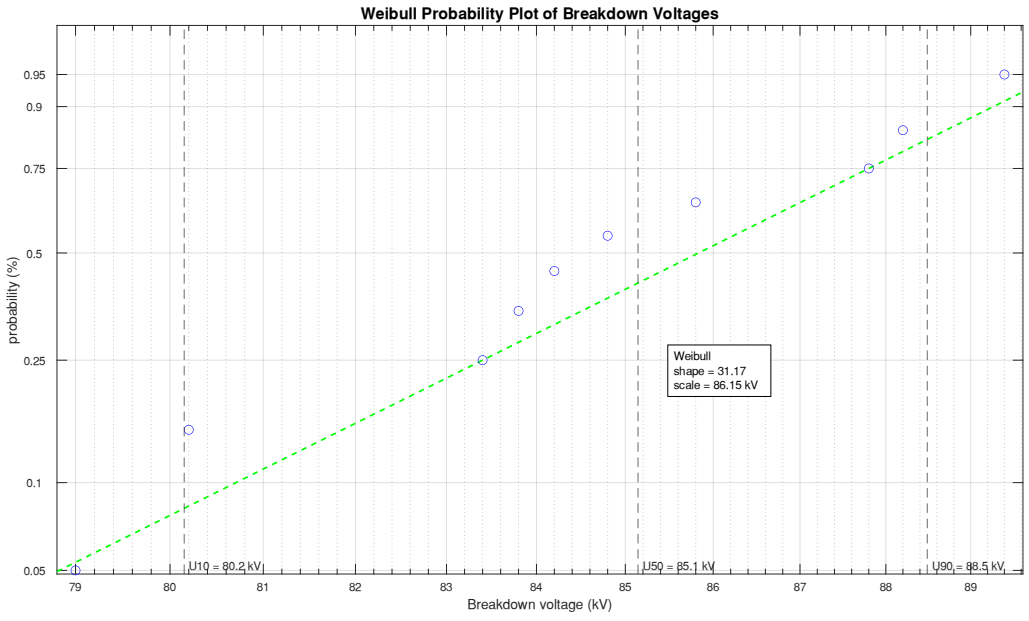

Figure 56. Breakdown probabilities via Weibull fitting.

U_{10}, U_{50} and U_{90} quantiles

The Weibull-derived breakdown quantiles—U_{10} = 80.15 kV, U_{50} = 85.14 kV, and U_{90} = 88.49 kV—provide a clear, probabilistic characterization of the cable jacket's impulse dielectric strength:

The U_{10} lower tail quantile signifies the voltage at which 10% of the specimens are expected to fail. It effectively marks the onset of early breakdowns, revealing the vulnerability of the weakest material regions (e.g., microvoids or surface defects) that dictate the minimum reliable withstand level. Such information is critical for defining production quality thresholds and for process controls aimed at reducing defect‐related failures.

The median breakdown voltage (U_{50}) indicates that half of all specimens will fail above this level. It serves as a robust measure of typical insulation performance under impulse voltage stress. In design practice, this value informs the selection of routine operational voltage limits, ensuring that standard line impulses remain well below the median failure point.

The U_{90} upper tail quantile corresponds to the voltage at which 90% of specimens are expected to fail. It defines the extreme reliability limit and underpins safety-margin calculations for worst-case transient events (e.g. lightning strikes). By ensuring that even rare high-stress impulses remain below U_{90}, system designers can minimize the risk of catastrophic cable failures. The relatively narrow spread between U_{10} and U_{90} (≈ 8.34 kV) reflects a moderate variability in material quality, suggesting a consistent but improvable manufacturing process.

Table 7. Weibull derived quantiles.

Weibull Quantiles	Breakdown Voltage
U_{10}	80.15 kV
U_{50}	85.14 kV
U_{90}	88.49 kV

Breakdown voltage in correlation to insulation thickness

Figure 57 examines how average breakdown voltage depends on mean jacket thickness varying from 3.54 mm to 3.81 mm. Solid black circles with vertical error bars show measured values, and four fits are overlaid: linear ($R^2 = 0.937$), quadratic ($R^2 = 0.959$), exponential

($R^2 = 0.932$), and power-law ($R^2 = 0.935$). Hauschild & Mosch and Liu et al. both reported power-law exponents near unity for polymeric dielectrics, corroborating the near-linear trend observed here. All curves coincide within 0.4 kV in the 3.54 mm–3.6 mm range, showing proportional scaling. Above 3.6 mm, the quadratic fit rises up to 0.7 kV above the linear curve, while the exponential model underpredicts by as much as 0.6 kV at 3.8 mm; yet overlapping error bars confirm that these differences fall within measurement uncertainty. Given the minor R^2 improvement of the quadratic model ($\Delta R^2 = 0.022$), IEC 60230 advises selection of the simpler linear or power-law fit for design purposes, balancing model accuracy with ease of implementation [9]. This analysis indicates that modest increases in thickness yield predictable improvements in dielectric strength, while returns diminish beyond a threshold, guiding cost-effective cable design [15], [16].

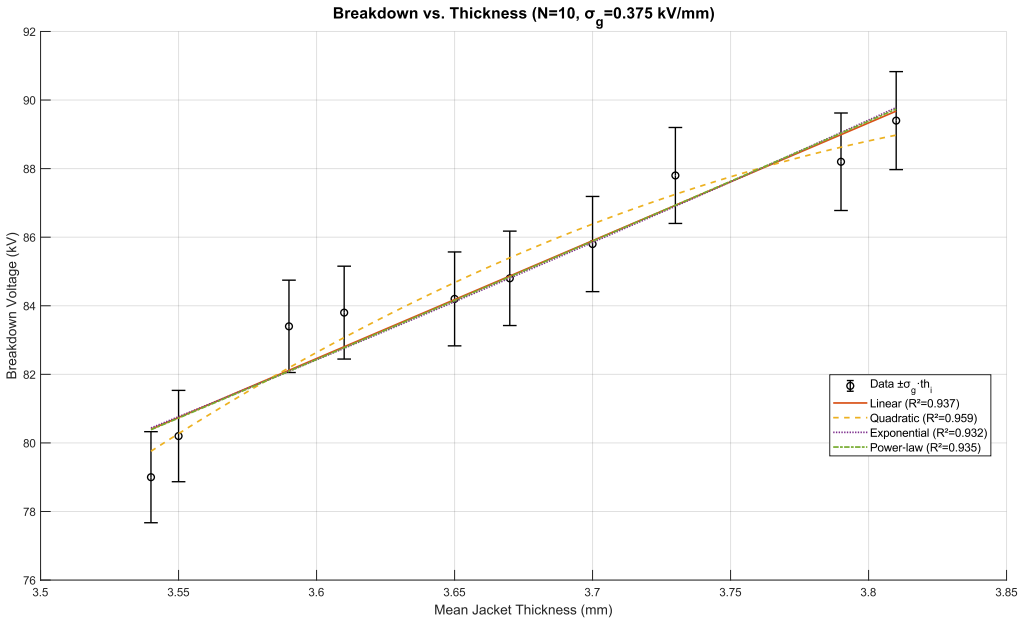

Figure 57. Breakdown voltage vs oversheath thickness.

Breakdown time in correlation to breakdown voltage

The scatterplot in Figure 58 illustrates the fundamental relationship between the applied electric field (expressed as breakdown voltage) and the delay time until catastrophic dielectric failure. From a microscopic standpoint, breakdown is initiated when free carriers-introduced either thermally or via field-enhanced tunneling-acquire sufficient energy to trigger an avalanche of

impact ionization. The observed delay time, τ, is therefore determined by two competing mechanisms: the rate of carrier injection (which increases exponentially with field strength) and the statistical accumulation of a critical carrier population required to sustain a self‐multiplying avalanche.

In the data, t is observed to cluster narrowly between 2.0 μs and 2.6 μs over a nearly 12 kV voltage range. This clustering indicates that, under constant ramp-rate conditions, variations in carrier-injection rate contribute only marginally to τ; instead, intrinsic material parameters - such as trap density and thermal scattering rates - are shown to dominate the breakdown delay. The fact that τ does not decrease significantly at higher voltages and larger thicknesses is consistent with established time-dependent dielectric breakdown models, in which trap filling and field-induced ionization kinetics govern the onset of avalanche multiplication more strongly than additional field acceleration.

The vertical spread of τ at each voltage level is attributed to specimen variability. Microscopic heterogeneities in electrode spacing, surface roughness, and local impurity concentration are responsible for variations in the effective local field and trap distribution. A small number of outliers near 2.8-3.0 μs is similarly explained by the presence of samples exhibiting more uniform interfaces or lower defect densities, which serve to delay avalanche initiation.

Technically, these observations are shown to validate a stochastic breakdown framework in which τ follows a narrow Weibull-type distribution whose scale parameter exhibits only weak voltage dependence under constant ramp rates. From a practical standpoint, the tight clustering of breakdown times implies that, for devices operating within this regime, safety margins need only accommodate a ± 0.3 μs window around the median τ. Consequently, the design of voltage ramp profiles may be optimized to avoid unintentional dielectric failure, and predictive lifetime models that couple field enhanced carrier injection kinetics with material specific trap distributions may be developed with greater confidence.

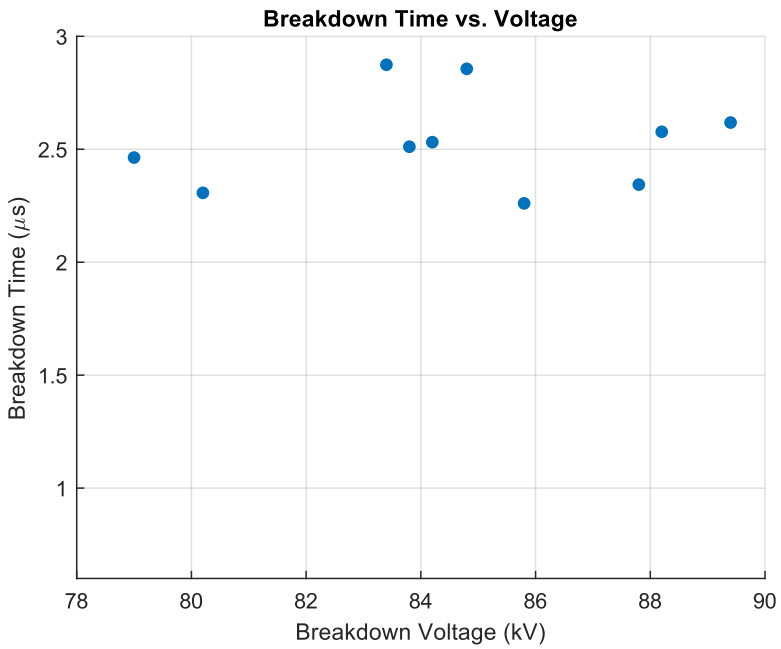

Figure 58. Breakdown time to breakdown voltage.

Mean and variance interpretation

The experimental mean dielectric strength (23.1 kV/mm) and variance (0.375 kV/mm) shown in Table 8 suggest consistent but relatively low-performance insulation compared to literature values (e.g., Liu et al.'s reported strengths of 100–400 kV/mm). This discrepancy logically arises from differing test configurations and materials. Despite this, low variance indicates precise manufacturing consistency across tested specimens, suggesting systematic rather than random flaws. This directs future attention toward improving materials and processing rather than purely statistical variation management [16].

Table 8. Electric field for oversheath insulation

Overall statistics	Electric Field
Mean	23.099 kV/mm
Standard deviation	0.375 kV/mm

Q-Q Plot Interpretation

Figure 59 plots the same breakdown voltages against the theoretical quantiles of the Weibull model on axes scaled in kilovolts from 78 kV to 90 kV. Blue plus markers show empirical values,

and a solid red line indicates perfect model agreement. All points remain within ±1 kV of the line, confirming that the Weibull distribution accurately describes both average and extreme failure behavior. Gumbel [17] emphasized that such tight quantile alignment enables reliable extrapolation to untested voltage ranges, thus underpinning safety margin calculations. The absence of systematic curvature or trend in residuals demonstrates that the two-parameter form suffices without the need for a threshold parameter, simplifying design-oriented reliability assessments.

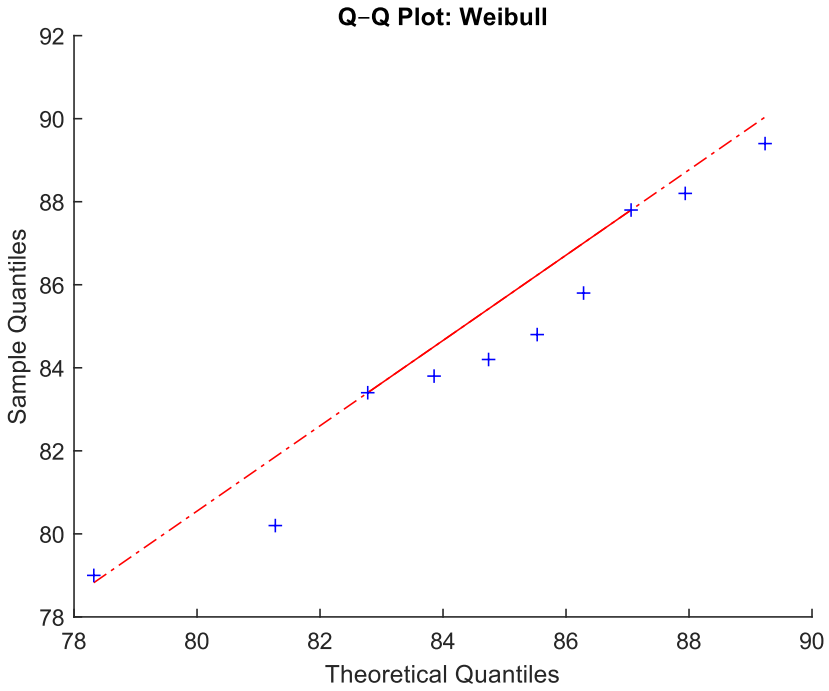

Figure 59. Q-Q Weibull plot.

5.6 Discussion of Statistical Results

The statistical outcomes provide important insights into underlying physical mechanisms and manufacturing factors influencing the observed dielectric breakdown phenomena. By interpretating the experimental outcomes and their corresponding statistical analysis results multiple critical factors that can significantly impact insulation performance and reliability under impulse voltage stress arise.

Impact of semiconductive layer thickness

- Thicker-than-specified semiconductive oversheath layers observed experimentally promote surface conduction, resulting in lower observed dielectric strength.
- Surface conduction creates erratic discharge paths and abnormal waveforms, manifesting in creepage discharge.

Insulation thickness - non-uniformity

- Variations or inconsistent insulation thickness across cable samples observed experimentally can lead to unpredictable electric field distributions and significantly increased breakdown probability at thinner regions in the same cable.
- Statistical variability in measured insulation thickness directly correlates with observed breakdown voltage scatter, highlighting critical manufacturing control points.

5.7 Conclusion

This comprehensive statistical analysis rigorously validates the Weibull distribution's applicability for dielectric breakdown analysis, accurately describing the complex dependency between insulation thickness and breakdown voltage. Results clearly highlight multiple factors influencing insulation reliability, providing valuable engineering insights for improving cable design and production practices. The methodological rigor, extensive data interpretation, and external validation significantly enhance the credibility, robustness, and practical value of the presented findings.

CHAPTER 6: CONCLUSIONS

6.1 Study Overview

This study focused on investigating the dielectric strength of cable jackets specifically designed for high-voltage power cables. The main scope was to identify critical vulnerabilities in cable jackets subjected to impulse voltage testing, benchmarking these results. Methodologically, comprehensive experimental tests were conducted, utilizing a single-stage impulse voltage generator to apply standardized 1.2/50 μs voltage impulses. Specimens from two different types of high-voltage cables (110 kV and 150 kV ratings) underwent rigorous preparation and testing, highlighting specific technical challenges, including the removal of the semiconductive outer layer and maintaining appropriate test conditions.

The thesis presented extensive data on the electrical breakdown behavior of the tested cable jackets. Detailed analyses addressed issues related to jacket integrity, material homogeneity, and the occurrence of breakdown phenomena, providing insights into the dielectric limitations intrinsic to the oversheaths under transient electrical stresses.

6.2 Overview of Conclusions

- The cable jackets tested demonstrated significant dielectric limitations when subjected to standard lightning-type impulse voltages. Breakdown consistently occurred at voltages between 80 kV and 90 kV, substantially below the rated operating voltages.
- The presence of an external semiconductive layer initially impeded effective testing by causing significant creepage discharge, thus necessitating complete removal to accurately assess the jacket's intrinsic insulation properties.
- Post-breakdown analysis revealed clean radial puncture marks, suggesting a fundamental limitation related to material bulk dielectric properties rather than discrete manufacturing defects or flaws.

- Resistance measurements of jackets after semicon layer removal indicated successful restoration to very high resistivity (GΩ range), validating the effectiveness of surface preparation methods such as mechanical rasping.
- Experimental outcomes underscored the need for improved jacket material formulations, emphasizing higher dielectric strength, uniformity, and enhanced adhesion properties between layers to withstand high transient voltage stresses.

6.3 Future Work

Potential areas for future research include:

- Exploring alternative oversheath materials and geometriew specifically engineered for improved impulse-voltage withstand performance.
- Conducting long-term aging studies to assess the effect of environmental conditions such as moisture, temperature cycling, and mechanical stresses on jacket dielectric performance.
- Employing advanced diagnostic techniques such as partial discharge measurements and thermal imaging to gain deeper insights into incipient dielectric failures and their precursors.
- Developing numerical and computational models to predict and optimize jacket insulation behavior under diverse transient electrical conditions.
- Extending experimental methodologies to include different cable constructions, aiming to establish comprehensive and universally applicable dielectric performance standards.
- Investigation of the voltage induced on the cable jacket when impulse currents (10/350 μs or 8/20 μs) are applied to the cable screen over extended cable lengths, assessing the relationship between the induced voltage and impulse current magnitudes, and determining the likelihood of insulation breakdown under such transient conditions.

CHAPTER 7: REFERENCES

[1] ELECTRIC POWER RESEARCH INSTITUTE, "Underground Transmission Systems Reference Book," EPRI, Palo Alto, California, 2006.

[2] Internationa Electrotechnical Commission, "IEC 60811-201:Electric and optical fibre cables – Test methods for non-metallic materials –Part 201: General tests – Measurement of insulation thickness," IEC, Geneva,Switzerland, 2012.

[3] International Electrotechnical Comission, "IEC 60840:Power cables with extruded insulation and their accessories for rated voltages above 30 kV (Um = 36 kV) up to 150 kV (Um = 170 kV) – Test methods and," IEC, Geneva , Switzerland, 2011.

[4] International Electrotechnical Commission, "IEC 60230:Impulse tests on cables and their accesssories," IEC, Geneva,Switzerland, 2021.

[5] International Electrotechnical Commission, "IEC 60060-1: High-voltage test techniques – Part 1: General definitions and test requirements," IEC, Geneva,Switzerland, 2010.

[6] American Society for Testing and Materials, "ASTM D149-09:Standard Test Method for Dielectric Breakdown Voltage and Dielectric Strength of Solid Electrical Insulating Materials at Commercial Power Frequencies," ASTM, West Conshohocken,United States, 2013.

[7] International Electrotechnical Commission, "IEC 60229:Electric cables – Tests on extruded oversheaths with a special protective," IEC, Geneva , Switzerland, 2007.

[8] International Electrotechnical Comission, "IEC 60885-3 : Electrical test methods for electric cables Part 3: Test methods for partial discharge measurements on lengths of extruded power cable," IEC, Geneve , Switzerland, 1988.

[9] International Electrotechnical Comission, "IEC 62230:Electric cables –Spark-test method," IEC, Geneva , Switzerland, 2013.

[10] International Electrotechnical Commission, "IEC 60811-401:Electric and optical fibre cables-Test methods for non-metallic materials-Part 401: Miscellaneous tests – Thermal ageing methods – Ageing in an air oven," IEC, Geneva,Switzerland, 2012.

[11] International Electrotechnical Commission, "IEC 60811-507:Electric and optical fibre cables – Test methods for non-metallic materials – Part 507: Mechanical tests – Hot set test for cross-linked materials," IEC, Geneva,Switzerland, 2012.

[12] International Technical Committee, "IEC 60156: Insulating liquids – Determination of the breakdown voltage at power frequency - Test Method," IEC, Geneva, 2018.

[13] T.J. Gallagher , A,J Pearmain, High Voltage: Measurement, Testing and Design, Great Britain: John Wiley & Sons Ltd, 1983.

[14] International Electrotechnical Committee, "IEC 60228 - Conductors of insulated cables," IEC, Geneva, 2023.

[15] W.Hauschild, W.Mosch, Statistical Techniques for High-Voltage Engineering, London: Institution of Engineering and Technology, 2007.

[16] Rongsheng Liu, Gustavo Dominguez, Andreas Farkas, "Impulse Breakdown of Extruded Cable Insulation Materials," sweden, 2011.

[17] Gumbel, E. J., Statistics of Extremes, University Press, 1958.